Article

Cell Reports

Dopamine Autoreceptor Regulation of a Hypothalamic Dopaminergic Network

Graphical Abstract

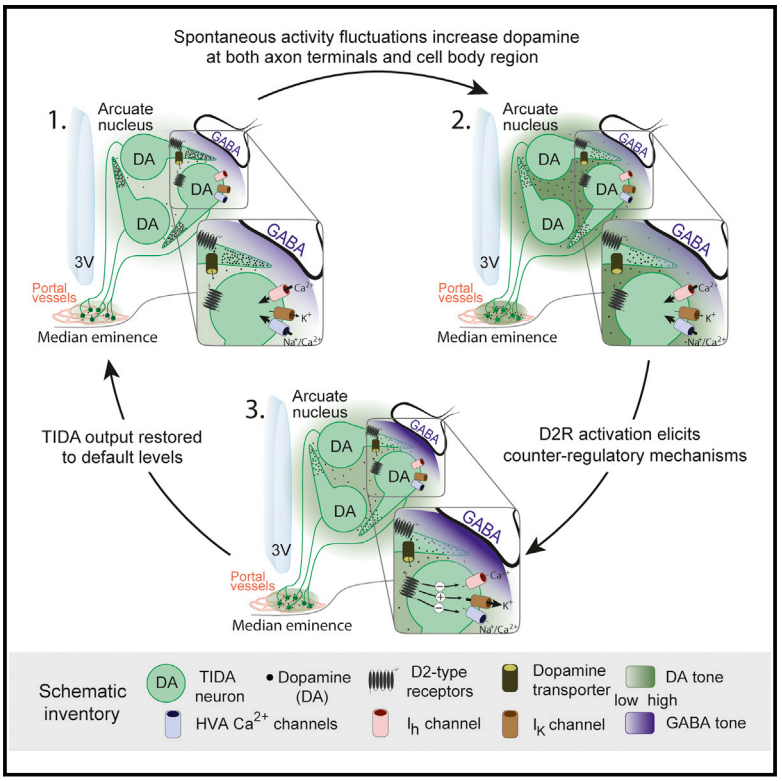

Highlights

- Frequency tuning by autoreceptors occurs in an oscillating dopamine neuron network
- Dopamine reuptake and D2 receptors at the cell-body level determine frequency
- Oscillation is controlled through the combination of pre- and postsynaptic actions

Authors

Stefanos Stagkourakis, Hoseok Kim, David J. Lyons, Christian Broberger

Correspondence

stefanos.stagkourakis@ki.se (S.S.), christian.broberger@ki.se (C.B.)

In Brief

Stagkourakis et al. describe an ultra-short feedback loop in hypothalamic rat dopamine (TIDA) neurons. Using electrophysiology, they show that TIDA network oscillations are tuned to ambient levels of dopamine. This homeostatic regulation, involving complementary sets of pre- and postsynaptic mechanisms, may contribute to the hormonal side effects of antipsychotics.

Stagkourakis et al., 2016, Cell Reports *15*, 735–747
April 26, 2016
http://dx.doi.org/10.1016/j.celrep.2016.03.062

Cell Reports
Article

Dopamine Autoreceptor Regulation of a Hypothalamic Dopaminergic Network

Stefanos Stagkourakis,[1,*] Hoseok Kim,[1] David J. Lyons,[1,2] and Christian Broberger[1,*]
[1]Department of Neuroscience, Karolinska Institutet, 171 77 Stockholm, Sweden
[2]Present address: The Rowett Institute of Nutrition and Health, Greenburn Road, Bucksburn, Aberdeen AB21 9SB, UK
*Correspondence: stefanos.stagkourakis@ki.se (S.S.), christian.broberger@ki.se (C.B.)
http://dx.doi.org/10.1016/j.celrep.2016.03.062

SUMMARY

How autoreceptors contribute to maintaining a stable output of rhythmically active neuronal circuits is poorly understood. Here, we examine this issue in a dopamine population, spontaneously oscillating hypothalamic rat (TIDA) neurons, that underlie neuroendocrine control of reproduction and neuroleptic side effects. Activation of dopamine receptors of the type 2 family (D2Rs) at the cell-body level slowed TIDA oscillations through two mechanisms. First, they prolonged the depolarizing phase through a combination of presynaptic increases in inhibition and postsynaptic hyperpolarization. Second, they extended the discharge phase through presynaptic attenuation of calcium currents and decreased synaptic inhibition. Dopamine reuptake blockade similarly reconfigured the oscillation, indicating that ambient somatodendritic transmitter concentration determines electrical behavior. In the absence of D2R feedback, however, discharge was abolished by depolarization block. These results indicate the existence of an ultra-short feedback loop whereby neuroendocrine dopamine neurons tune network behavior to echoes of their own activity, reflected in ambient somatodendritic dopamine, and also suggest a mechanism for antipsychotic side effects.

INTRODUCTION

Dopamine neurons play a pivotal role in several brain functions, including cognition, reward, and motor output (Jentsch et al., 1997; Servan-Schreiber et al., 1998; Reeves et al., 2005; Katz, 1979; Lippa et al., 1973; Graeff, 1966; Andén and Strömbom, 1974; Westermann and Staib, 1976). Changes in dopamine activity have been implicated in, e.g., schizophrenia, addiction, and Parkinson disease (Stevens et al., 1974; Seeman, 2013; Compton et al., 1996; Ungless et al., 2010; Södersten et al., 2014; Chase et al., 1974). A physiologically appropriate dopamine output depends, to a great extent, on homeostatic mechanisms. These mechanisms are only partly understood but includes immediate feedback through autoreceptors (Cragg and Greenfield, 1997).

Dopamine is also an important signaling molecule in the hypothalamus, where it inhibits prolactin release from the anterior pituitary (Freeman et al., 2000). The main source of neuroendocrine dopamine is the tuberoinfundibular dopamine (TIDA) neurons, located in the dorsomedial hypothalamic arcuate nucleus (dmArc). TIDA neurons release dopamine into the portal capillaries at the median eminence (ME) for transport to the anterior pituitary gland (Lyons and Broberger, 2014). Patterned dopaminergic inhibition within the lactotrophic axis is essential for successful reproduction, as evidenced by the impaired fertility and other sexual side effects associated with the hyperprolactinaemia commonly seen in patients treated with antipsychotics with dopamine antagonist properties (Holt and Peveler, 2011).

The pituitary consequences of TIDA neuron activation are well established (Fuxe, 1963). However, the actions of dopamine on TIDA neurons have been the subject of only a few studies and remain poorly understood. Biochemical studies have indicated that TIDA neurons may be under inhibitory influence by dopamine receptors of the type 2 family (D2R) (Berry and Gudelsky, 1991; Lin et al., 2000; Liang et al., 2014), but other investigators have found no effect (Demarest and Moore, 1979a; Timmerman et al., 1995) or even disinhibition via D2R (Durham et al., 1996). How autoreceptors affect TIDA membrane properties and network activity has not been studied. In the ventral tegmental area (VTA) and the substantia nigra (SN) of the midbrain, where this issue has been studied in more depth, autoinhibition appears to protect dopamine neurons from runaway excitation (Björklund and Lindvall, 1975; Aghajanian and Bunney, 1977; Paladini et al., 2003; Beckstead et al., 2004; Gentet and Williams, 2007). This has been shown to involve D2R-mediated activation of hyperpolarizing K^+ conductances (Silva and Bunney, 1988). TIDA neurons share several features with their mesencephalic counterparts, including co-transmitters, such as GABA (Everitt et al., 1984) and neurotensin (Ibata et al., 1983), and the ability to exhibit both tonic and phasic discharge configurations. It is not known, however, whether mechanisms of autoregulation are similar or different in TIDA cells.

Intriguingly, recent in vitro studies have revealed that TIDA neurons in the male rat discharge in an oscillating pattern, which can be switched to tonic discharge by hormones and neurotransmitters (Lyons et al., 2010, 2012; Briffaud et al., 2015) that, in in vivo studies, have correlated to prolactin release and lactation. This phenomenon raises the question of whether and

how dopamine participates in the maintenance of this rhythmic behavior. The important question of how an oscillating circuit tunes its activity to internal feedback is poorly understood and ideally studied in a spontaneously active preparation. Furthermore, understanding the homeostatic regulation of TIDA neurons is clinically important, as several of the most troubling side effects associated with antipsychotic, as well as antidepressant, drugs derive from their ability to raise serum prolactin (Madhusoodanan et al., 2010; Serretti and Chiesa, 2011). The results we present here suggest the existence of a ultra-short autoinhibitory loop in TIDA neurons encompassing both pre-and postsynaptic mechanisms that is continuously adjusted to ambient somatodendritic dopamine levels.

RESULTS

Dopamine D2R Activation Decreases Oscillation Frequency

The TIDA neurons in the male rat exhibit stereotyped electrophysiological properties, including anomalous inward rectification, an A-like current conductance, and a slow (0.05–0.07 Hz) oscillation. This electrical profile correlates to the expression of tyrosine hydroxylase and can reliably be used to identify these cells for in vitro recordings (Lyons et al., 2010). Using these criteria, we first sought to determine how TIDA network behavior is affected by agonists of the dopamine receptors, using whole-cell recordings.

Application of dopamine (20 μM) induced a reversible increase of the oscillation cycle duration (+7.66 ± 1.47 s; n = 5; $p < 0.05$ versus control; ANOVA; Figures 1Ba–1Bd; Table S1). To identify the different components of the cycle, a custom written analysis program was developed (Figure 1A; Supplemental Experimental Procedures). Thus, the dopamine-induced slowing of the oscillation was found to result primarily from an increase in phase 1 (i.e., initial slow depolarization from nadir: +5.03 ± 1.13 s; n = 5; $p < 0.05$ versus control; ANOVA; Figure 1Bb; Table S1) but also from a smaller increase in phase 3 duration (spiking phase: +2.92 ± 0.71 s; n = 5; $p < 0.05$ versus control; ANOVA; Figure 1Bb; Table S1). The duration of phases 2 (fast depolarization) and 4 (repolarization) were not affected by the application of dopamine. Application of the non-selective dopamine receptor agonist apomorphine (20 μM) resulted in similar changes in oscillation cycle properties, as seen with dopamine (n = 5/5; Figures 1Ca–1Cd; Table S1).

Application of the D2R agonist, 20 μM quinpirole (Qp) also caused changes to oscillation parameters indistinguishable from those observed following dopamine application (n = 8/8; Figure 1E; Table S1). In the presence of the D1-type-receptor (D1R)-specific agonist, SKF-81,297 (10 μM) (Reavill et al., 1993), however, oscillation parameters were not significantly altered (n = 5/5; Figure 1D; Table S1). As it could not, at this point, be excluded that ongoing dopamine release in the slice might be acting on D1 receptors diminishing an effect of exogenous agonists (Dewey et al., 1992), we also tested the D1R antagonist, SCH-23,390 (10 μM) (Bourne, 2001), but prolonged application of this compound did not affect oscillation parameters (n = 7/7; Table S1). Last, we tested whether D2R activation alters rhythmicity in the presence of fast-ionotropic blockade (FIB) (100 μM picrotoxin [Ptx], 10 μM CNQX, and 25 μM AP-5). In these conditions, 20 μM Qp led to a prolongation of cycle duration (5.99 ± 0.91 s; n = 6; $p < 0.01$ versus FIB) by increasing phase 1 and phase 3 durations (Figure S2; Table S1). These data identify D2R as an autoreceptor that modulates TIDA membrane properties and slows down network rhythm.

D2R Antagonism Switches TIDA Neurons to Depolarization Block

These findings raised the question of whether there is ongoing D2R activation due to endogenous dopamine release in the spontaneously active slice. This issue was addressed by pharmacological antagonism of the D2R. Application of the selective D2R antagonist eticlopride (1 μM) resulted in a depolarization of the TIDA oscillation nadir (+2.46 ± 0.77 mV; n = 5; $p < 0.05$ versus control; Figures 2Aa and 2Ab; Table S1) concomitant with a decrease in phase 1 duration (−1.88 ± 0.65 s; n = 5; $p < 0.05$ versus control; Figure 2Ab; Table S1) and an increase of phase 3 duration (+1.51 ± 0.37 s; n = 5; $p < 0.05$ versus control; Figure 2Ab; Table S1). The cycle duration remained unchanged (−0.64 ± 0.56 s; n = 5; $p > 0.05$ versus control; Figure 2Ab; Table S1), as predicted by the opposite changes in the duration of phases 1 and 3. Application of a second D2R antagonist, the typical antipsychotic haloperidol (1 μM), had similar effects (n = 5/5; Figures 2Ba and 2Bb; Table S1). Closer examination of the individual action potentials (APs) revealed that application of either eticlopride or haloperidol induced a statistically significant decrease in amplitude and broadening of the APs (Figures 2Ad and 2Bd; Table S2). This effect on amplitude and half-width increased in size from the first to the fifth AP (Figures 2Ad and 2Bd; Table S2). The effect on the waveform of the fifth AP of a cycle is demonstrated in Figures 2Ac and 2Bc.

Similar changes in AP waveform have previously been described in midbrain dopamine neurons as a prodrome of the depolarization block (DB) (Bikson et al., 2003; Vandael et al., 2015; Richards et al., 1997) induced by antipsychotics (Grace and Bunney, 1986). This similarity, and the depolarized nadir induced by eticlopride, prompted us to examine the effects of higher concentrations of the D2R antagonists. Application of eticlopride (10 μM, n = 5/5) or haloperidol (10 μM, n = 11/11) resulted in a gradual depolarization and ultimate collapse of the oscillation (Figures 2Ca and 2Cb). AP amplitude gradually decreased and was eventually followed by a complete loss of APs concurrent with the collapse of the oscillation (Figures 2Ca and 2Cb). Injection of depolarizing square current pulses resulted only in a single, low-amplitude AP, verifying that the capacity for regenerative firing was compromised (Figure 2Cc). Collectively, these results suggest that TIDA neurons respond to D2R antagonists by excitation, leading to DB in a manner highly similar to what has been described in midbrain dopamine neurons following chronic application of dopamine antagonist antipsychotics (Grace and Bunney, 1986).

Dopamine Reuptake at the Cell-Body Level Regulates TIDA Oscillations

The partly opposite effects of D2R agonists and antagonists suggest that the baseline behavior of TIDA neurons may

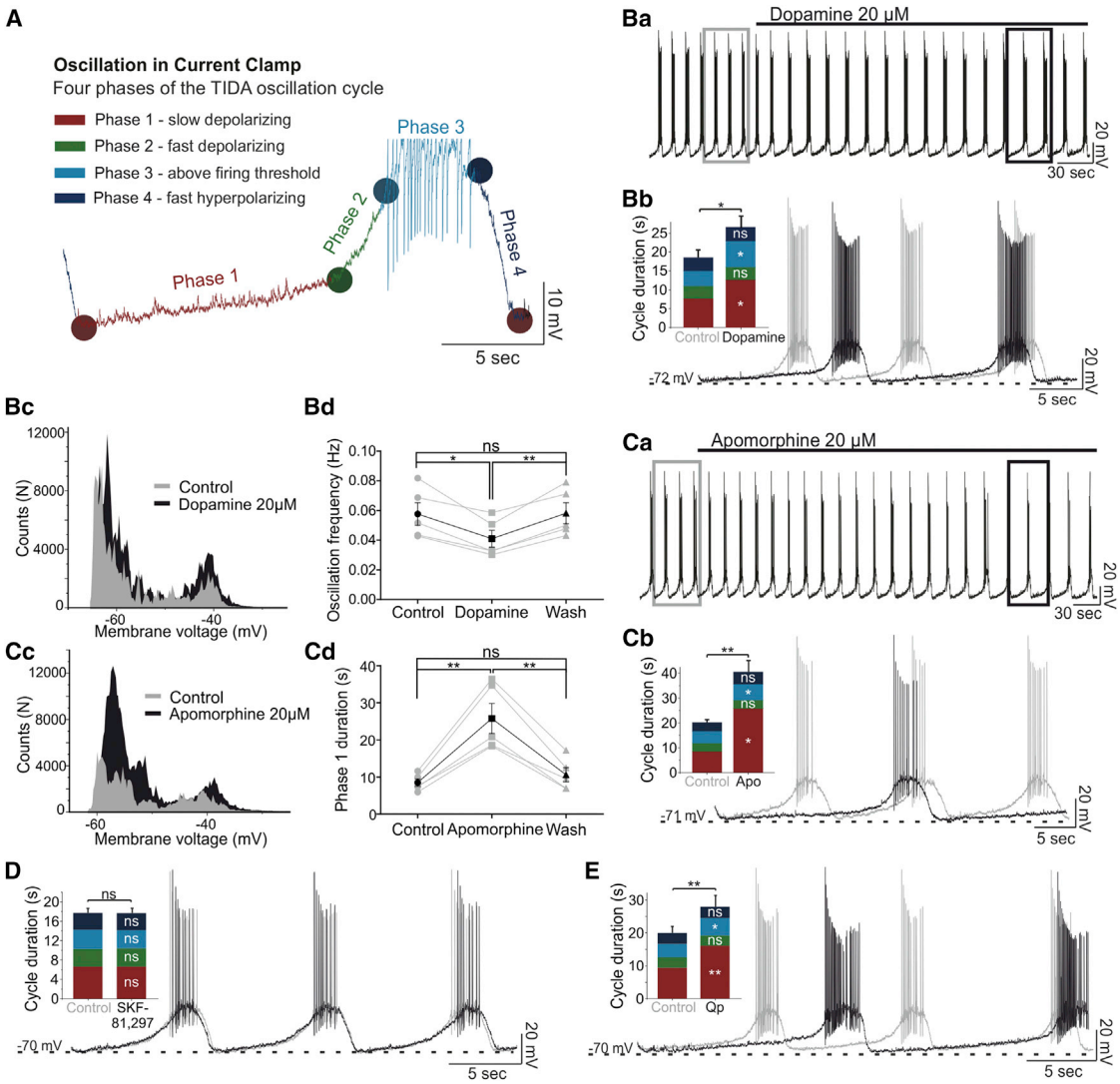

Figure 1. D2R Activation Decreases TIDA Neuron Oscillation Frequency

(A) Current-clamp recording from TIDA neuron illustrating one cycle of the oscillation divided into four phases based on changes in slope (dV/dt).

(Ba–Bd) In (Ba), dopamine application leads to a reversible decrease in oscillation frequency (−0.017 ± 0.004 Hz, $p < 0.05$, $n = 5$). (Bb) Expanded and overlaid boxed traces from (Ba) (gray trace indicates control, black trace indicates dopamine), and population data show a large increase in phase 1 duration (+5.03 ± 1.13 s) and a smaller increase in phase 3 duration (+2.92 ± 0.71 s; $p < 0.05$; $n = 5$). (Bc) Membrane voltage distribution plot illustrates accentuated biphasic distribution in the presence of dopamine. (Bd) Histogram demonstrating a reversible decrease of the oscillation frequency by dopamine.

(Ca–Cd) Organized as in (Ba)–(Bc), (Ca)–(Cc) illustrate a similar slowing effect on oscillation by apomorphine as by dopamine; increases in phase 1 (+17.28 ± 3.09 s) and phase 3 (+1.76 ± 0.56 s) duration ($p < 0.05$, $n = 5$). Apomorphine-induced accentuation of biphasic membrane voltage distribution as shown in (Cc). (Cd) Histogram demonstrating a reversible increase in phase 1 duration by apomorphine.

(D and E) Organized as in (Ba). (D) Application of the D1R-agonist, SKF-81,297, does not alter cycle or phase durations ($n = 5$). (E) Application of the D2R receptor agonist, Qp ($n = 8$), decreases oscillation frequency (−0.013 ± 0.001 Hz; $p < 0.0001$) and increases the duration of phases 1 (+6.61 ± 1.76 s; $p < 0.01$) and 3 (+1.23 ± 0.38 s; $p < 0.05$). Note similarity to dopamine and apomorphine effects (Ba, Bb, Ca, and Cb).

ns, not significant.

depend on continuous dopaminergic feedback. To further explore endogenous dopamine release in the dmArc we investigated the effect of blocking the dopamine transporter (DAT). The existence of the DAT in the TIDA system is controversial. Evidence has been presented for both the absence (Demarest and Moore, 1979b; Annunziato et al., 1980) and existence (Demaria et al., 2000; Bossé et al., 1997) of functional dopamine reuptake in these cells. We addressed this issue directly by applying a DAT blocker, either GBR-12783 or methylphenidate, and recorded the electrophysiological response. In the presence of GBR-12783 (1 μM) and methylphenidate (50 μM), TIDA neurons exhibited changes similar to those elicited by D2R agonists, i.e., dopamine, apomorphine, and Qp, and slowed down oscillation frequency (GBR-12783, n = 8/8;

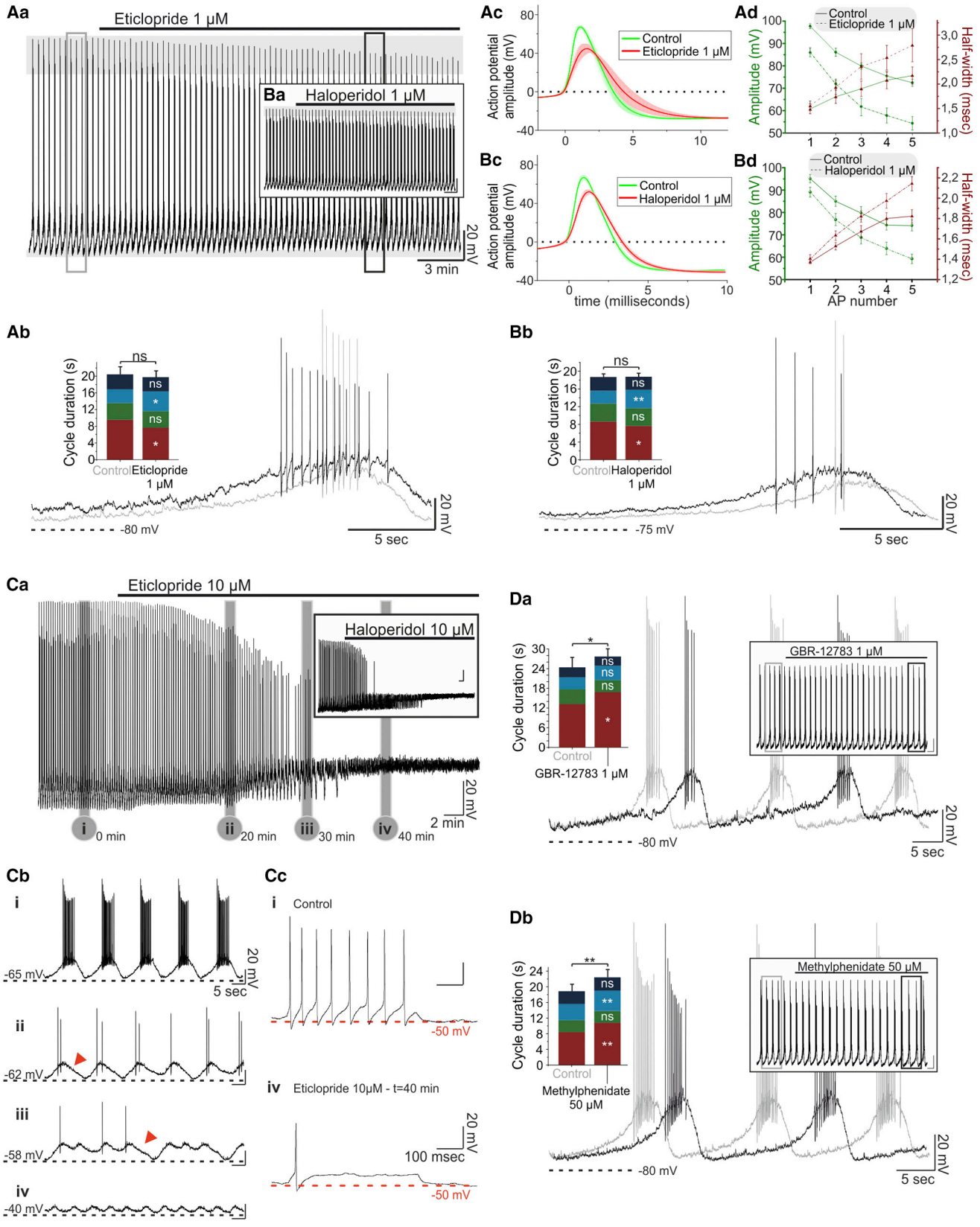

(legend on next page)

methylphenidate, n = 5/5; Figures 2Da and 2Db; Table S1). While both phases 1 and 3 were significantly prolonged in the presence of methylphenidate, the application of GBR-12783 only resulted in a significantly increased duration of phase 1. These data suggest the existence of endogenous release of dopamine from TIDA neurons and the presence of functional dopamine reuptake at the somatic level in these cells. Next, we sought to identify the membrane actions that underlie the D2R-mediated modulation of TIDA neurons.

D2R Activation Causes a Cs^+-Sensitive Hyperpolarization

Application of tetrodotoxin (TTX; 0.5 μM) abolishes the TIDA oscillation (Lyons et al., 2010) likely owing to the inhibition of a persistent Na^+ current. Under these conditions, and with membrane potential set to −60 mV via negative current injection, application of Qp (20 μM) resulted in a hyperpolarization of −4.19 ± 0.78 mV (n = 6; $p < 0.01$ versus control; Figures 3A and 3C). This hyperpolarization was attenuated when Qp was applied to cells recorded with an intracellular solution containing Cs^+ ($p < 0.05$ versus Qp) (−1.69 ± 0.45mV; n = 9; $p < 0.05$ versus control; Figures 3A–3C). While Cs^+ is known to block h current (I_h), the ability of intracellularly applied Cs^+ to attenuate this current is controversial (Harris and Constanti, 1995). Thus, to more specifically test whether the phase 1 prolongation by D2R activation is partly an effect involving I_h, Qp was co-applied with the I_h blocker ZD-7288 (10 μM). Under these conditions, application of Qp failed to significantly increase phase 1 duration, whereas a prominent prolongation of phase 3 remained (Figures 3D and 3E). These findings suggest a D2R-mediated decrease of I_h.

D2R Agonism Inhibits an Inward Current Operating at High Voltage

To characterize the ionic currents modulated by D2R agonism, TIDA neurons were recorded in voltage-clamp mode in the presence of TTX (0.5 μM) at a holding potential (V_{Hold}) of −60 mV, i.e., at which the Qp-induced hyperpolarization had been observed. Application of Qp (20 μM) did not significantly affect holding current under these conditions (−0.49 ± 1.5 pA; n = 6; $p > 0.05$ versus control; Figure 3F). To determine current changes that might occur throughout the membrane potential spectrum, a voltage-clamp ramp protocol of 500-ms durations was used, allowing the identification of D2R-mediated currents throughout the voltage spectrum of −115 mV to 0 mV (Figure 3Ga). Digital subtraction of the ramp performed with control versus Qp (Figure 3Gb) revealed a Qp-induced current (I_{Qp}) that was a non-reversing net outward current, active only at membrane potentials positive of approximately −45 mV (n = 5; Figure 3Gc), increasing with depolarization within the range tested (V_{Hold} = 0 mV; +124.83 ± 34.97 pA). At a V_{Hold} negative of −50 mV no prominent I_{Qp} is evoked, suggesting that the Cs^+-sensitive current underlying the phase 1 depolarization (discussed earlier) is not of sufficient amplitude to be isolated under these conditions.

D2R Activation Inhibits High-Voltage-Activated Ca^{2+} Channels in TIDA Neurons

The I_{Qp} may reflect the activation of an outward current and/or the inhibition of an inward current. As the I-V relationship of I_{Qp} is similar to that of a reversed I_{Ca}^{2+} (Nowycky et al., 1985; Fedulova et al., 1985), we tested whether D2R stimulation decreased Ca^{2+} flux in TIDA neurons, using a voltage ramp protocol.

Application of Qp (20 μM) was followed by a substantial and significant decrease of the high-voltage-activated (HVA) Ca^{2+} currents (−52.71 ± 9.09 pA; n = 7; $p < 0.01$ versus control; Figure 4A). Control experiments did not identify a prominent low-voltage-activated, T-type Ca^{2+} current in TIDA neurons (Figure 4A). Application of the L-type-specific blocker nimodipine (10 μM), however, attenuated the Ca^{2+} current (−62.8 ± 19.04 pA; n = 5; $p < 0.05$ versus control, ANOVA; Figure 4B). Under L-type Ca^{2+} channel blockade, the Qp-induced decrease in HVA current was significantly diminished (−34.6 ± 9.42 pA; n = 5; $p < 0.05$ versus nimodipine, ANOVA; Figure 4B). Application of the N-type-specific Ca^{2+} channel blocker ω-conotoxin GVIA (1 μM) decreased the Ca^{2+} currents (−71.4 ± 22.72 pA; n = 5; $p < 0.05$ versus control, ANOVA; Figure 4C). Under N-type Ca^{2+} channel blockade, application of Qp (20 μM) resulted in a small, but significant, decrease of the remaining Ca^{2+} current (−7.8 ± 1.91 pA; n = 5; $p < 0.05$ versus control, ANOVA; Figure 4C). Last, upon co-application of nimodipine and ω-conotoxin GVIA, the Ca^{2+} current decreased dramatically (−119.4 ± 6.94 pA; n = 5; $p < 0.001$ versus control, one-way ANOVA; Figure 4D). In these conditions, application of Qp (20 μM) failed to induce a significant decrease of the remaining Ca^{2+} current (−10.6 ± 5.32 pA; n = 5; $p > 0.05$ versus control, ANOVA; Figure 4D).

Figure 2. D2R Antagonism and DAT-Blockade Effect on TIDA Neurons

(Aa–Ad) In (Aa) and (Ab), a current-clamp recording from oscillating TIDA neuron is shown. Application of eticlopride (1 μM) is followed by a progressive decrease in AP amplitude and depolarization of the nadir (horizontal gray bars). Boxed sections from (Aa) are expanded and overlaid in (Ab) (gray indicates control; black indicates eticlopride), with population data shown in the histogram; note the decrease in the phase 1 duration (−1.88 ± 0.65 s) and the increase in the phase 3 duration (+1.51 ± 0.37 s) ($p < 0.05$, n = 5). (Ac) Averaged (indicated by solid lines, SE in shading) APs in the absence (green) and presence (red) of 1 μM eticlopride. (Ad) Average AP amplitude (green) progressively decreases and half-width (red) increases during the oscillation cycle in the presence of 1 μM eticlopride (indicated by a dashed line; solid line indicates control).

(Ba–Bd) Organized as in (Aa)–(Ad), respectively, these panels illustrate the similarity of effects of 1 μM haloperidol and eticlopride.

(Ca–Cc) In (Ca), following application of 10 μM eticlopride, TIDA neurons progressively depolarize, with the oscillation ultimately collapsing and AP firing being abolished (n = 5/5). Inset shows the same effect with 10 μM haloperidol (n = 11/11). (Cb) Boxed sections in (Ca) are expanded in (Cb i)–(Cb iv). (Cc) Voltage responses to step current pulses in control (Cb i) and after a 40-min application of 10 μM eticlopride (Cb iv) show a loss of capacity for repetitive discharge.

(Da and Db) Effect of DAT antagonists on oscillation frequency. (Da) Application of GBR-12783 (1 μM) prolongs cycle duration (3.49 ± 1.25 s; n = 8; $p < 0.05$ versus control) via phase 1 prolongation (3.64 ± 1.41 s; n = 8; $p < 0.05$ versus control). (Db) Similarly, methylphenidate increases cycle duration (2.62 ± 0.44 s; n = 5; $p < 0.01$ versus control) via phase 1 (+2.38 ± 0.38 s) and, to a smaller extent, phase 3 (+1.06 ± 0.18 s) ($p < 0.01$, n = 5).

ns, not significant.

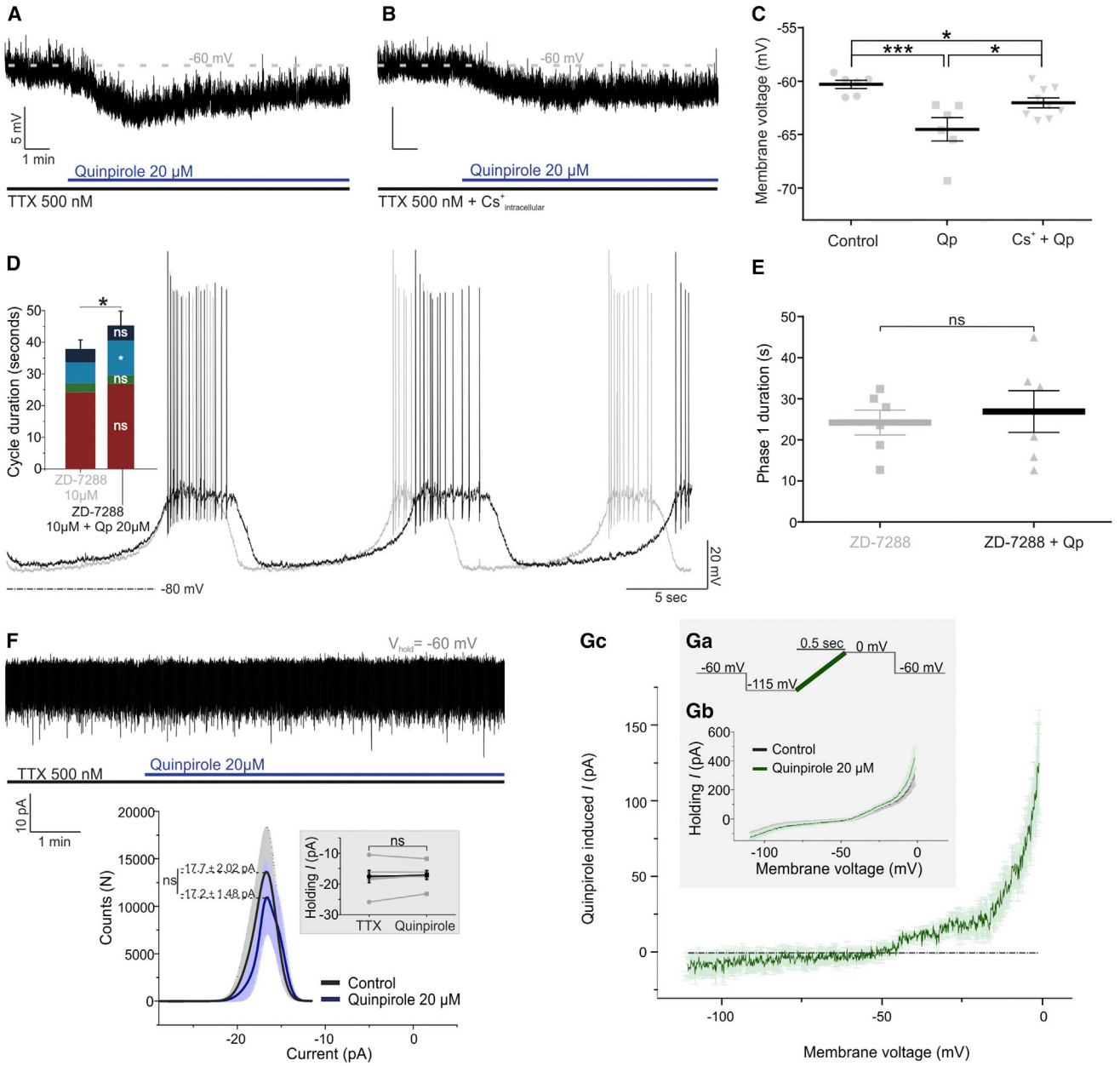

Figure 3. D2R Activation Induces a Postsynaptic Outward Current Operating at a Depolarized Membrane Potential

(A) Current-clamp recording of a TIDA neuron in the presence of TTX to abolish oscillation and APs. Note hyperpolarization following application of Qp.

(B) Recording under the same conditions as in (A) but with cesium methanesulfonate included in the intracellular solution; note the attenuation of Qp-induced hyperpolarization.

(C) Average membrane potential in control, with Qp applied (−4.19 ± 0.78 mV; n = 6; $p < 0.01$), and Qp applied in the presence of intracellular cesium (−1.69 ± 0.45 mV; n = 9; $p < 0.01$).

(D) Current-clamp recording of a TIDA neuron in the presence of ZD-7288 and co-application of Qp. Under these conditions, cycle duration increase is attributable exclusively to phase 3 prolongation (4.25 ± 1.38 s; n = 6; $p < 0.05$ versus ZD-7288).

(E) D2R activation under I_h blockade does not lead to phase 1 prolongation (2.67 ± 3.3 s; n = 6; $p > 0.05$ versus ZD-7288).

(F) Voltage-clamp recording of a TIDA neuron in the presence of TTX at a holding potential of −60 mV. Under these conditions, Qp does not significantly affect membrane current (−0.49 ± 1.5 pA; n = 6; $p > 0.05$). Population data in the inset show control in black and Qp in blue (solid lines indicate average; shaded area indicates SE.

(Ga–Gc) Inset shows voltage-clamp ramps: −115 to −0 mV; 500-ms (Ga–Gc) recordings of TIDA neurons in the absence (black) and presence (blue) of Qp (averaged traces; (Gb) n = 5). (Gc) Qp-induced current. Note the minimal current flowing between −115 and −50 mV and large inward current activated at depolarized voltage (> −50 mV).

ns, not significant.

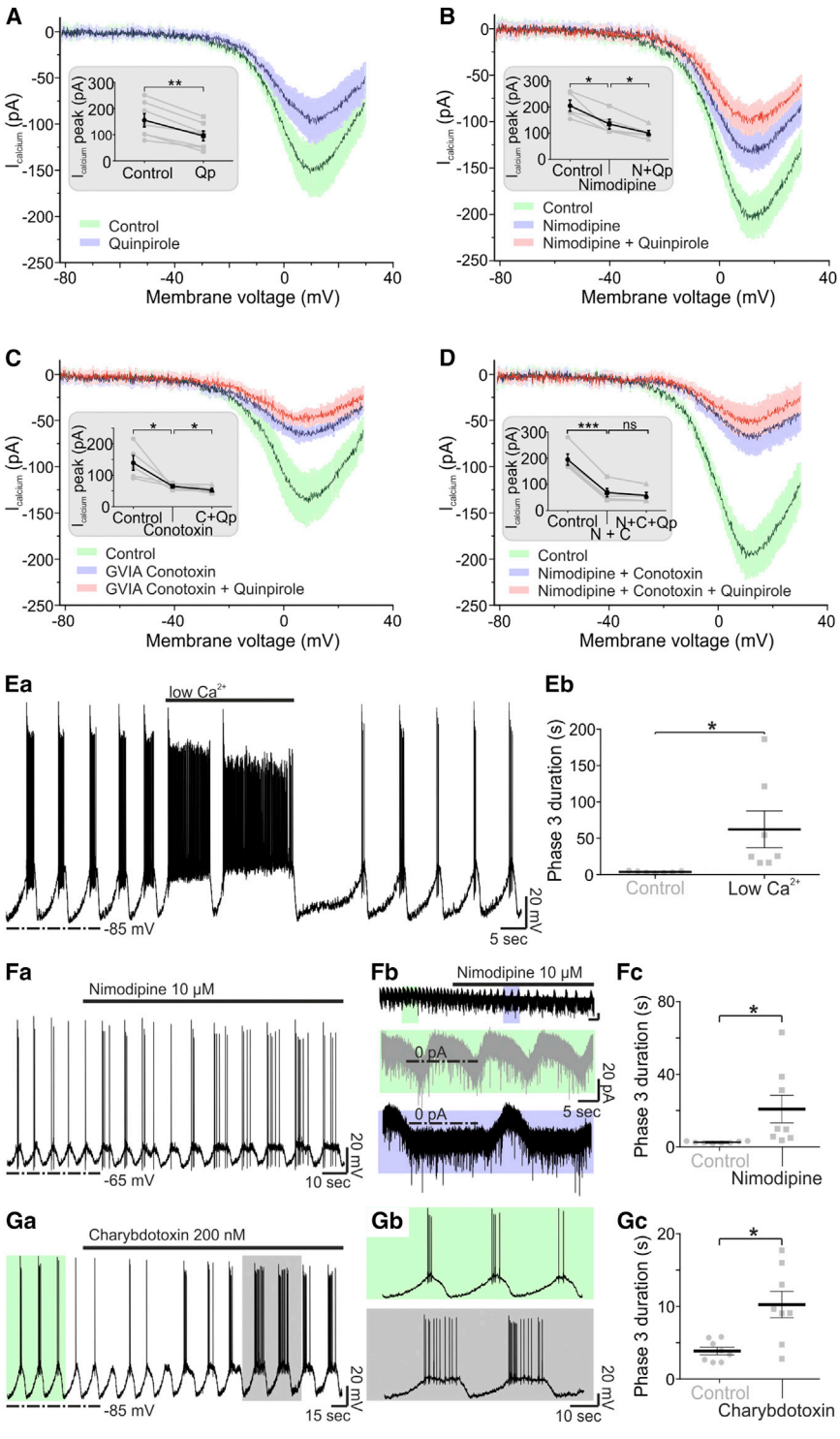

Figure 4. D2R Activation Decreases Ca^{2+} Currents in TIDA Neurons through L- and N-Type Ca^{2+} Channels

(A) Average voltage-clamp ramp traces recorded from TIDA neurons (ns = 7/5/5/5 for A–D, respectively) under pharmacological isolation of Ca^{2+} currents. Current recorded under control conditions shown in green (solid lines, average; shaded area, SE). Note the attenuation of HVA Ca^{2+} currents in the presence of Qp (blue). Inset shows average current at peak in control (154.9 ± 25.44 pA) and upon Qp application (102.1 ± 19.10 pA, n = 7, $p < 0.01$ versus control).

(B) Organized as (A), but with recording in the presence of the L-type HVA current antagonist, nimodipine (blue), and nimodipine and Qp co-applied (red). The control HVA Ca^{2+} current (205 ± 21.55 pA) is decreased following the application of nimodipine (142.2 ± 18.78 pA, n = 5, $p < 0.05$ versus control), upon which Qp has a diminished effect (107.6 ± 10.49 pA; n = 5; $p < 0.05$ versus nimodipine).

(C) Organized as in (A), but with recording in the presence of the N-type HVA current antagonist, GVIA-conotoxin (blue), and GVIA-conotoxin and Qp co-applied (red). The control HVA Ca^{2+} current (141.2 ± 22.77 pA) is decreased by application of GVIA-conotoxin (69.8 ± 4.55 pA; n = 5; $p < 0.05$ versus control), upon which Qp has a miniature yet significant effect (62 ± 5.54 pA; n = 5; $p < 0.05$ versus GVIA-conotoxin).

(D) Organized as in (A), but with recording in the presence of nimodipine and GVIA-conotoxin (blue) and of nimodipine, GVIA-conotoxin, and Qp co-applied (red). The control HVA Ca^{2+} current (194.2 ± 21.55 pA) is markedly decreased when both L- and N-type channels are blocked (74.8 ± 16.18 pA; n = 5; $p < 0.001$ versus control). Under these conditions, application of Qp does not further decrease HVA currents (64.2 ± 11.56 pA; n = 5; $p > 0.05$ versus GVIA-conotoxin and nimodipine). Data are presented in absolute values.

(Ea and Eb) Effect of (Ea) "low-Ca^{2+}" aCSF on the TIDA oscillation and (Eb) phase 3 duration, which is increased (59.98 ± 24.45 s; n = 7; $p < 0.05$ versus control).

(Fa–Fc) Current-clamp (Fa) and voltage-clamp (Fb) recordings in the presence of nimodipine, demonstrating (Fc) phase 3 prolongation (18.33 ± 7.61 s; n = 8; $p < 0.05$ versus control).

(Ga–Gc) In (Ga), a current-clamp recording is shown in the presence of the BK channel blocker, charybdotoxin (200 nM). (Gb) Recording in (Ga), shown in higher temporal resolution; control (light green) versus charybdotoxin (gray). Note the prolongation of phase 3 and discharge. (Gc) BK channel blockade leads to a significant prolongation of phase 3 (6.41 ± 1.85 s; n = 8; $p < 0.05$ versus control).

ns, not significant.

Interplay of BK Channels and Ca^{2+} Influx Controls Phase 3

To assess whether this D2R-mediated decrease in L-type Ca^{2+} currents could prolong phase 3 duration, short applications of low-Ca^{2+}/high-Mg^{2+} artificial cerebrospinal fluid (aCSF) were performed. A reversible phase 3 prolongation was demonstrated under these conditions (59.98 ± 24.45 s; n = 7; $p < 0.05$ versus control; Figures 4Ea and 4Eb). Similarly, application of nimodipine resulted in prolongation of phase 3 (18.33 ± 7.61 s; n = 8; $p < 0.05$ versus control) in current-clamp (n = 4) as well

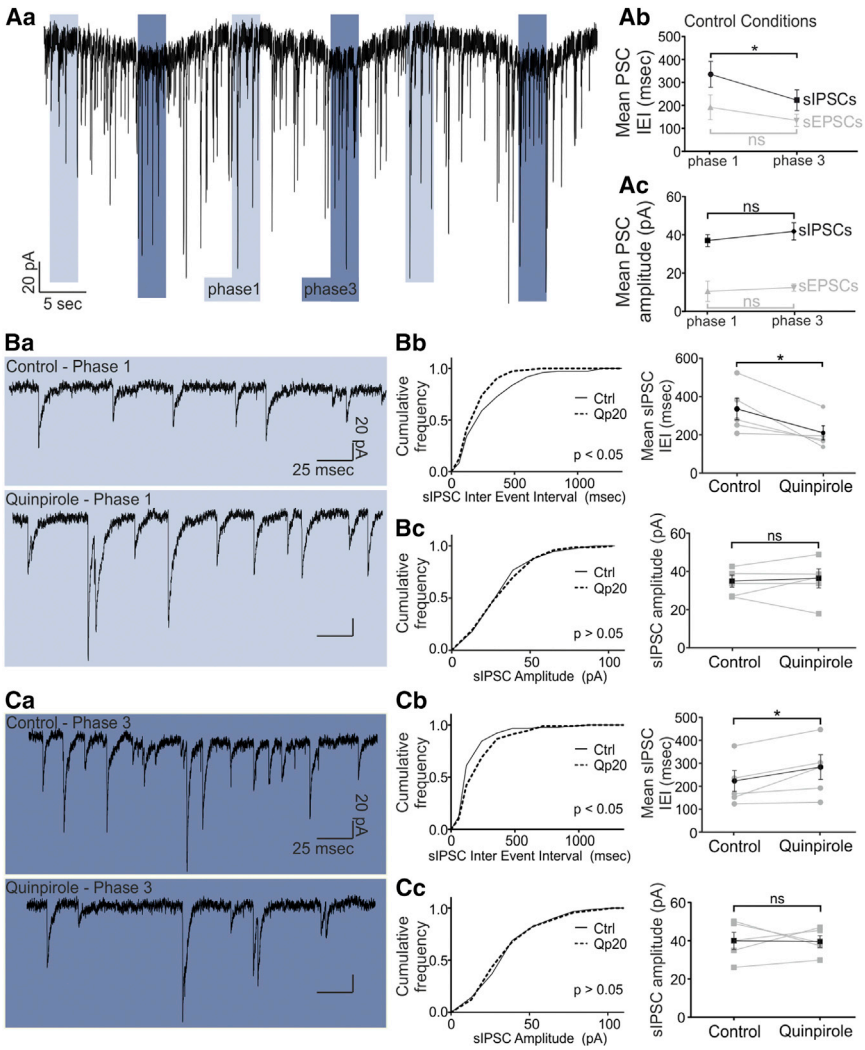

Figure 5. Phase-Dependent Modulation of sIPSC Frequency via D2R Agonism

(Aa–Ac) In (Aa), a voltage-clamp recording from TIDA neurons is shown, in the presence of ionotropic glutamate receptor antagonists and using high $[Cl^-]_i$ to isolate sIPSCs. Phase 1 is indicated by light blue, and phase 3 is indicated by dark blue. (Ab) The sIPSC IEI is significantly lower in phase 3 than in phase 1 (−112.5 ± 32.55 ms; n = 5; $p < 0.05$), whereas the sEPSC IEI is not significantly different (−57.07 ± 30.5 ms; n = 6; $p > 0.05$). (Ac) The amplitude of sIPSCs (+4.81 ± 3.87 ms; n = 5; $p > 0.05$, phase 3 versus phase 1) and sEPSCs (+0.19 ± 0.46 ms; n = 6; $p > 0.05$) is not different between phases 1 and 3.

(Ba–Bc) In (Ba), raw voltage-clamp phase 1 traces are shown in the absence (top) and presence (bottom) of Qp. (Bb) Cumulative frequency distribution of the sIPSC IEI, demonstrating a significant increase in sIPSC frequency (−125.0 ± 40.09 ms; KS-2 $p < 0.05$; t test $p < 0.05$; n = 5) during phase 1 after application of Qp. (Bc) Phase 1 sIPSC amplitude remains unchanged by Qp (+1.39 ± 3.19 pA; KS-2 $p > 0.05$; t test $p > 0.05$; n = 5).

(Ca–Cc) In (Ca), raw voltage-clamp phase 3 traces are shown in the absence (top) and presence (bottom) of Qp. (Cb) Cumulative frequency distribution of the sIPSC IEI demonstrating a decrease in sIPSC frequency (+60.43 ± 21.61 ms, KS-2 $p < 0.05$; t test $p < 0.05$; n = 5) during phase 3 in the presence of Qp. (Cc) Phase 3 sIPSC amplitude is not affected (−0.34 ± 4.75 pA; KS-2, $p > 0.05$; t test, $p > 0.05$; n = 5).

ns, not significant.

as voltage-clamp (n = 4) recordings (Figures 4Fa–4Fc). As Ca^{2+} influx through L-type channels has commonly been implicated in the activation of Ca^{2+}-dependent K^+ channels (e.g., (Marrion and Tavalin, 1998), we last applied the big conductance Ca^{2+}-activated K^+ channel (BK) antagonist, charybdotoxin (200 nM). In the presence of charybdotoxin, phase 3 was also significantly increased in duration (6.41 ± 1.93 s; n = 8; $p < 0.05$ versus control). These data suggest that TIDA D2R activation leads to inhibition of the L-type ($Ca_v1.1$-1.4) and N-type ($Ca_v2.2$) HVA Ca^{2+} channels accounting for the prolongation of phase 3, possibly via the interplay of Ca^{2+} and BK channels responsible for phase 3 termination.

D2R Phase-Dependent Modulation of Rhythmic Inhibitory Input

Next, we investigated whether, in addition to postsynaptic modulation of TIDA membrane currents, D2R stimulation also affects synaptic input to these neurons. The frequency of inhibitory synaptic input in TIDA neurons is higher in phase 3 than in phase 1 (Lyons et al., 2010) (Figures 5Aa–5Ac; phase 1: spontaneous inhibitory post-synaptic current (sIPSC) inter-event interval (IEI) = 335.5 ± 56.57 ms; phase 3: sIPSC IEI = 223 ± 45.18 ms; difference in means ± SEM, −112.5 ± 32.55 ms; $p < 0.05$; n = 5). This discrepancy may reflect different sources of inhibitory input onto TIDA neurons across the oscillatory cycle. IPSCs were, therefore, compared separately in phase 1 and phase 3. The IEI for sIPSCs in the presence of Qp (20 μM) was significantly decreased during phase 1 (−125 ± 40.09 ms; n = 5; Figures 5Ba and 5Bb; KS-2, $p < 0.05$ versus control; t test, $p < 0.05$ versus control; Figures 5Ba and 5Bb) but significantly increased during phase 3 (+60.43 ± 21.62 ms; n = 5; Figures 5Ca and 5Cb; KS-2, $p < 0.05$ versus control; t test, $p < 0.05$ versus control; Figures 5Ca and 5Cb). In contrast, the amplitude of sIPSC was not affected by Qp application during either phase 1 (+1.39 ± 3.19 pA; n = 5; Figure 5Bc; KS-2, $p > 0.05$ versus control; t test, $p > 0.05$ versus control; Figures 5Ba and 5Bc) or phase 3 (+0.34 ± 4.75 pA; n = 5; Figure 5Cc; KS-2, $p > 0.05$; t test, $p > 0.05$; Figures 5Ca and 5Cc). Analysis of spontaneous excitatory postsynaptic currents (sEPSCs) revealed no significant changes (Figure S3). Likewise, miniature IPSCs and EPSCs (recorded in the presence of 0.5 μM TTX) were affected neither in IEI nor in amplitude (Figure S4). Taken

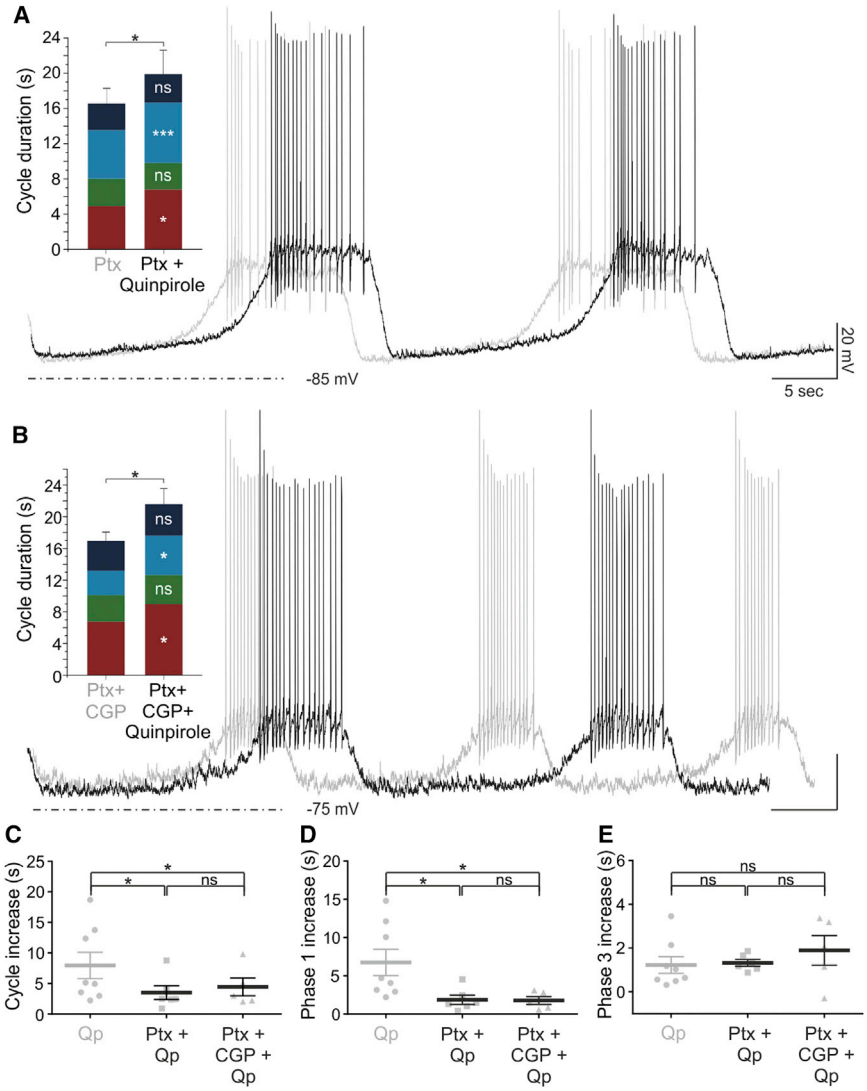

Figure 6. Increased $GABA_A$-Mediated Inhibition Contributes to D2R-Mediated Slowing of Oscillation Frequency by Extending Phase 1

(A) Overlaid current-clamp recordings from oscillating TIDA neuron in the presence of Ptx before (gray) and during (black) application of Qp. Activation of the D2R induces an increase in cycle duration (+3.49 ± 1.13 s; $p < 0.05$ versus Ptx; n = 6) by increasing the duration of phases 1 (+1.86 ± 0.59 s; $p < 0.05$ versus Ptx; n = 6) and 3 (+1.32 ± 0.15 s; $p < 0.001$ versus Ptx; n = 6).

(B) Experiment is as in (A), but with addition of CGP-55845 (CGP) in the bath to block $GABA_B$ receptors. When Qp is added, increases in the duration of the oscillation cycle (+4.43 ± 1.45 s; $p < 0.05$ versus Ptx + CGP; n = 5), phase 1 (+1.76 ± 0.51 s; $p < 0.05$ versus Ptx + CGP; n = 5), and phase 3 (+1.89 ± 0.68 s; $p < 0.05$ versus Ptx + CGP; n = 5) are seen also under these conditions. Scale bars, as shown in (A).

(C–E) Comparison of the increases in cycle (C), phase 1 (D), and phase 3 (E) duration induced by Qp application in control conditions (n = 7) versus during $GABA_A$ (n = 6) or combined $GABA_{A/B}$ (n = 5) blockade. (C) The increase in cycle duration following Qp alone (7.95 ± 2.17 s) is significantly larger than the increases seen in Ptx + Qp (3.49 ± 1.13 s; $p < 0.05$) and Ptx + CGP + Qp (4.43 ± 1.45 s; $p < 0.05$). In contrast, the increase measured in Ptx + Qp was not significantly different from the increase in Ptx + CGP + Qp. (D) Similarly, the increase in the duration of phase 1 following Qp alone (6.61 ± 1.76 s) is significantly greater than the increases seen for Ptx + Qp (1.86 ± 0.59 s; $p < 0.05$) and Ptx + CGP + Qp (2.22 ± 0.78 s; $p < 0.05$); increases recorded in Ptx + Qp and Ptx + CGP + Qp are not significantly different from each other. (E) The increases in the duration of phase 3 recorded in Qp (1.23 ± 0.38 s), Ptx + Qp (1.32 ± 0.15 s) and Ptx + CGP + Qp (1.89 ± 0.68 s) are not different from each other. ns, not significant.

together, these data suggest that D2R stimulation increases inhibitory input during phase 1, while it decreases it during phase 3.

$GABA_A$ Receptor Blockade Attenuates the D2R Activation Effect on Oscillation Frequency

The Qp-induced increase in sIPSC frequency during phase 1 suggests the possibility that the D2R-mediated decrease of oscillation frequency may be partly caused by augmented synaptic inhibition. If so, the effect of Qp on phase 1 should be diminished or abolished in the absence of $GABA_A$-mediated inhibition. Thus, Ptx (100 μM) was bath applied prior to Qp (20 μM) application. Under these conditions, the Qp-mediated increase in cycle duration via prolongation of phase 1 was diminished by 48% (Figures 6A and 6C–6E; n = 6). Importantly, the Qp-induced increase in phase 3 duration was not affected by Ptx application (Figure 6E; n = 6; $p > 0.05$). The combined blockade of $GABA_A$ (by Ptx) and $GABA_B$ receptors (by the antagonist, CGP-55845; 10 μM) did not produce any additional attenuation of the Qp-mediated increase in cycle period or phase 1 or 3 duration, compared to Ptx alone (n = 5; Figures 6B–6E; Table S1). These data demonstrate that increased $GABA_A$ transmission contributes to dopaminergic autoregulation of the TIDA oscillation frequency, acting within the same membrane potential spectrum as, and likely parallel to, a Cs^+-sensitive hyperpolarizing postsynaptic current (Figures 3A–3C).

DISCUSSION

Feedback regulation is a core feature of CNS circuits. In the neuroendocrine system, such regulation has generally been studied in the context of multicomponent feedback loops, involving actions of the corresponding pituitary hormone—or a peripheral target hormone—on the hypothalamic "master" population. In the lactotrophic axis, prolactin can stimulate both dopamine production (Clemens and Meites, 1968; Hökfelt and Fuxe, 1972; Demarest et al., 1986; Gonzalez et al., 1988) and AP discharge and waveform (Lyons et al., 2012; Brown et al.,

2012) in TIDA cells to increase the suppression of its own release in the pituitary. However, the possibility that parvocellular neurons can autoregulate their own activity, as a means of immediate homeostatic tuning, has received little attention. In gonadotropin-releasing-hormone (GnRH)-expressing neurons, there is evidence of an "ultra-short feedback loop" (Bedran de Castro et al., 1985) involving modification of the electrical activity (Xu et al., 2008). In TIDA neurons, the literature offers conflicting evidence for (Berry and Gudelsky, 1991; Liang and Pan, 2001) and against (Demarest and Moore, 1979a; Durham et al., 1997; Timmerman et al., 1995) the existence of autoreceptors. Importantly, the possibility that membrane properties and network activity are targeted by autoreceptors has not been explored on identified TIDA neurons.

Our experiments reveal that increasing D2R activation causes two coincident changes in the TIDA duty cycle: a prolonged duration of phase 1, resulting in a slower oscillation, followed by a minor prolongation of phase 3. The similar reconfiguration of the oscillation following the exogenous application of Qp, as when ambient endogenous dopamine was increased by GBR-12783 and methylphenidate induced DAT blockade (although the former prolonged only phase 1), strongly indicates that these effects are not simply pharmacological. It should be stressed that the present results do not unequivocally rule out dopaminergic sources other than TIDA neurons as the endogenous ligand source for autoreceptors. Indeed, the term "autoreceptor" commonly refers to a receptor whose ligand is produced by the same neuron; it does not, as such, posit that the ligand is exclusively supplied by that cell. However, given that the slice preparation used here likely includes little of dopamine populations outside of the A12 group, the results using receptor and DAT blockers favor the interpretation that TIDA neurons are capable of autoregulation.

Our results further suggest that DATs are located at release sites within the dmArc, i.e., where the cell bodies of TIDAs are located. The functional expression of DAT within the TIDA system has been controversial, with arguments presented both for its absence (Lookingland et al., 1987) and for its presence (Bossé et al., 1997; Demaria et al., 2000). However, this discussion has largely been based on the assumption that TIDA DATs are located on axon terminal release sites (i.e., in the ME). Therefore, the point in question may not be whether TIDAs have DATs but rather the site of the transporter's actions. Our finding in which somatic whole-cell electrophysiology responds to DAT blockade in the same manner as following D2R stimulation indicates that DAT may be present and functional also on release sites that target the TIDA cell-body region. The exact nature of such release sites remains to be elucidated. Ultrastructural studies have shown that recurrent axon collaterals from TIDA neurons do not appear to form synaptic contacts, but extensive dendrodendritic and somatic contacts exist among these cells (Piotte et al., 1985). This anatomical organization is thus consistent with local release of dopamine—from dendrites and/or non-synapse forming axon collaterals—in the service of autoregulation, analogous to what has been observed in the midbrain dopamine neurons (Björklund and Lindvall, 1975; Geffen et al., 1976; Ford et al., 2010).

The modulation of phases 1 and 3 by D2R stimulation is mediated via distinct effects. At a membrane potential of −60 mV, i.e., within the phase 1 range, D2R activation induces a hyperpolarization, suggesting the contribution of direct post-synaptic actions. The current underlying the relatively modest (albeit with an impact at the network level) hyperpolarization is difficult to extract in voltage-clamp gap-free or ramp recordings; in TIDA neurons, this has yet only been reported with currents inducing several-fold larger changes in membrane potential (Lyons et al., 2010, 2012; Briffaud et al., 2015). Pharmacological experiments, however, showed that the hyperpolarization is diminished by intracellular Cs^+, implicating an increased K^+ conductance and/or an inhibition of the hyperpolarization-activated cation current (I_h). Evidence for each has been reported from midbrain dopamine neurons (Lacey et al., 1987; Momiyama et al., 1993; Jiang et al., 1993). Here, the increase in phase 1 duration by D2R activation was abolished during I_h blockade, suggesting I_h as a mediator of the effect of D2R activation during phase 1.

An increased frequency of sIPSCs was also observed by D2R activation, raising the possibility that augmented phasic inhibition contributes to the slowing of this phase. Notably, the increase in the duration of phase 1 was significantly attenuated when Qp was applied during $GABA_A$ blockade (by Ptx). Thus, simultaneous increases in presynaptic inhibition and postsynaptic K^+ or I_h-mediated outward current underlie the changes in phase 1 that primarily account for the decreased frequency resulting from an increased dopaminergic tone. As TIDA neurons do not discharge during phase 1, the increased inhibitory input is likely generated by another local neuronal population.

Phase 3 occupies a relatively depolarized membrane potential space, overlapping with the changes in HVA Ca^{2+} currents that followed D2R activation in TIDA neurons. Previous work has suggested the existence of L-type Ca^{2+} currents in these cells (Lyons et al., 2012). Our results confirm this and reveal the presence of N-type Ca^{2+} channels in TIDA neurons; the existence of P/Q and R-type Ca^{2+} channels remains to be investigated. We show that reductions in both L- and N-type Ca^{2+} currents contribute to the HVA I_{Qp}. Attenuated inward currents may seem counterintuitive as an explanation for the extended depolarized plateau of phase 3. However, TIDA neurons also exhibit Ca^{2+}-dependent K^+ currents (Lyons et al., 2012), and pharmacological inhibition of $I_{K(Ca^{2+})}$ results in an increased duration of phase 3, as shown in Figure 4. Thus, the attenuation of HVA Ca^{2+} currents accounts for the prolonged depolarization and discharge during D2R autoreceptor activation in TIDA neurons, possibly due to a decreased activation the $I_{K(Ca^{2+})}$ that ultimately causes repolarization to the nadir. The decreased synaptic inhibition during phase 3 (Figure 5Ca), though it does not in itself significantly contribute to prolonging the depolarized state, may add a synergistic net excitatory influence.

The mechanisms we identify here suggest an additional level of control in the neuroendocrine system where TIDA neurons homeostatically tune their activity to variations in the ambient extracellular levels of dopamine at the somatodendritic compartment. As local dopamine volume transmission increases (mimicked by Qp administration or DAT inhibition), a compensatory slowing of the network rhythm is initiated. The D2R and DAT are critical

molecular components of this tuning. In addition, the gap junction connectivity between TIDA neurons (Lyons et al., 2010) may provide efficient transduction of the D2R-induced changes throughout the network.

Notably, Paladini et al. (2003) have shown that when midbrain dopamine neurons are depleted of dopamine, burst firing is lost, suggesting that this type of feedback tuning may have general relevance for how the discharge pattern is controlled in dopamine neurons. This ultra-short loop impacts on TIDA neurons in a manner less dramatic than that for the feedback relayed via prolactin; while prolactin shifts discharge into tonic firing (Lyons et al., 2012), dopamine—even at high concentrations—maintains TIDA neurons in an oscillatory configuration but restructures phase relationships. It may be speculated that, as the distance between the feedback signal (i.e., effector hormone versus inherent transmitter) and the controlled system increases, more radical correcting actions may be required, as deviations from the set point have lasted for a longer time. Curiously, some degree of continuous D2R-mediated feedback appears necessary for the system to discharge. Gradual diminishment of this signal, as mimicked with low doses of eticlopride and haloperidol, results in changes generally opposite to those induced by D2R stimulation combined with blunting of spikes. Higher doses and longer application of the antagonists results in depolarization block and collapse of the oscillation, rendering the cell incapable of repetitive spiking. The DB that we demonstrate in TIDA neurons is, in vital ways, similar to what can be observed in midbrain dopamine neurons (Grace and Bunney, 1986) and has been proposed to provide a physiological mechanism that constrains a cell's firing frequency within a limited range, adding low-pass filter properties to a system (Wong et al., 2013).

Finally, our findings have clinical implications. Haloperidol and other antipsychotic drugs with D2R blocking properties at concentrations below the effective therapeutic dose cause hyperprolactinemia (Gruen et al., 1978), and associated reproductive dysfunctions such as impotence, menstrual disturbances, and infertility, commonly resulting in drug withdrawal (Serretti and Chiesa, 2011). This effect is usually attributed to haloperidol relieving pituitary lactotrophs of the tonic hyperpolarizing influence of D2R activation (MacLeod and Lehmeyer, 1974). The present results indicate, however, that dmArc TIDA autoreceptors may also contribute to such hyperprolactinemia by mediating D2R-antagonist-induced DB, causing the cessation of discharge and attenuated or abolished dopamine release in the portal vessels and removing inhibition from the lactotrophs. Thus, parallel actions of haloperidol at the somatodendritic level and at the endocrine target in the pituitary may underlie the reproductive side effects of D2R-active antipsychotic drugs. Thus, DB may be a mechanism that underlies not only the therapeutic actions of antidopaminergic antipsychotics (Grace et al., 1997) but also the adverse sexual effects commonly caused by these drugs.

In conclusion, our results using a spontaneously active neuroendocrine dopaminergic preparation reveal an ultra-short feedback pathway. These data suggest a rapid and continuous tuning of membrane rhythm to the circuit's own activity echoed in fluctuations of ambient somatodendritic levels of transmitter, and mediated by a combination of pre- and post-synaptic actions. This arrangement may be important both for maintaining physiologically appropriate prolactin levels and for the development of neuroleptic-induced reproductive side effects.

EXPERIMENTAL PROCEDURES

Acute slices of the mediobasal hypothalamus were prepared from 21- to 31-day-old male Sprague-Dawley rats (Charles River Laboratories). All animal experiments had received previous approval from the local ethical board, Stockholm's Norra Djurförsöksetiska Nämnd, and were performed in accordance with the European Communities Council Directive of November 24, 1986 (86/609/EEC). Slices were cut on a vibratome to 250-μm thickness and continuously perfused with oxygenated aCSF containing (in millimolar): 127 NaCl, 2.0 KCl, 1.2 NaH_2PO_4, 26 $NaHCO_3$, 1.3 $MgCl_2$, 2.4 $CaCl_2$, and 10 D-glucose, at room temperature during recording, unless stated otherwise. To identify the role of Ca^{2+} on oscillation parameters, "low-Ca^{2+}" extracellular recording solution was used (in millimolar): 127 NaCl, 1.9 KCl, 1.2 NaH_2PO_4, 26 $NaHCO_3$, 4.5 $MgSO_4$, 0.15 $CaCl_2$, and 10 D-glucose. Each slice was exposed only to a single bath application of pharmacological compounds and was used for a single experiment. Whole-cell current- and voltage-clamp recordings were performed with micropipettes filled with intracellular solution containing (in millimolar), 140 K-gluconate, 10 KCl, 10 HEPES, 10 EGTA, and 2 Na_2ATP (pH 7.3) (with KOH), unless stated otherwise. Recordings were performed using a Multiclamp 700B amplifier, a DigiData 1440 digitizer, and pClamp10.2 software (Molecular Devices). Slow and fast capacitative components were automatically compensated. Access resistance was monitored throughout the experiments, and neurons in which the series resistance exceeded 15 MΩ or changed $\geq$20% were excluded from the statistics. Liquid junction potential was 16.4 mV and not compensated. The recorded current was sampled at 10 kHz and filtered at 2 kHz. Recordings were performed using a Multiclamp 700B amplifier, a DigiData 1440 digitizer, and pClamp10.2 software (Molecular Devices). To control for any effect on the oscillation due to long-time recording intervals, we performed recordings of up to 100 min without adding any drug (Figure S1); rhythmic behavior was maintained, and cycle duration did not change significantly over time. For details on in vitro electrophysiology, see Supplemental Experimental Procedures.

Statistical Analysis

Data analysis was performed with GraphPad Prism 6, Clampfit software (Molecular Devices), AxoGraph, OriginPro 8 (OriginLab), and custom written MATLAB scripts. Phase analysis for each recording was based on data obtained over five consecutive oscillation cycles. Control traces were collected after 10 min of baseline and immediately followed by drug application. Postsynaptic currents were analyzed using Mini Analysis 6.0.9 (Synaptosoft). Detection threshold was set at 3-fold the root-mean-square (RMS) noise level, which typically was 3–6 pA. Frequency, inter-event interval, and amplitudes were calculated as a mean of the values obtained during a 60-s recording period. For postsynaptic current phase analysis, 3-s samples of phase 1 and 1-s samples of phase 3 of three consecutive oscillation cycles were compared in control versus drug. The two-sample Kolmogorov-Smirnov (KS-2) test was used to compare pooled cumulative frequency distributions of each component in the absence versus the presence of quinpirole. Statistical significance was set at $p < 0.05$ and was determined using the appropriate two-tailed Student's t test unless otherwise stated. Where it is stated that ANOVA was used, a one-way ANOVA was performed with the Bonferroni test in post hoc analysis. All data are presented as means ± SEM. Significance levels are indicated as: * = $p < 0.05$; ** = $p < 0.01$; and *** = $p < 0.001$.

SUPPLEMENTAL INFORMATION

Supplemental Information includes Supplemental Experimental Procedures, four figures, and two tables and can be found with this article online at http://dx.doi.org/10.1016/j.celrep.2016.03.062.

AUTHOR CONTRIBUTIONS

S.S., D.J.L., and C.B. designed experiments. S.S. performed experiments and analysis. D.J.L. performed experiments presented in Figures 4E–4G. H.K. assisted with MATLAB code. S.S. and C.B. wrote the manuscript.

ACKNOWLEDGMENTS

The authors thank Drs. Gilberto Fisone, Jessica Ausborn, Abdel El Manira, Gilad Silberberg, and members of the C.B. laboratory for advice, as well as Paul Williams for expert help with the graphical abstract. This study was supported by a Starting Investigator Grant from the ERC (ENDOSWITCH 261286), the Swedish Research Council (2010-3250), Novo Nordisk Fonden, and the Strategic Research Programme in Diabetes at Karolinska Institutet.

Received: November 22, 2015
Revised: February 17, 2016
Accepted: March 16, 2016
Published: April 14, 2016

REFERENCES

Aghajanian, G.K., and Bunney, B.S. (1977). Dopamine"autoreceptors": pharmacological characterization by microiontophoretic single cell recording studies. Naunyn Schmiedebergs Arch. Pharmacol. *297*, 1–7.

Andén, N.E., and Strömbom, U. (1974). Adrenergic receptor blocking agents: effects on central noradrenaline and dopamine receptors and on motor activity. Psychopharmacology (Berl.) *38*, 91–103.

Annunziato, L., Leblanc, P., Kordon, C., and Weiner, R.I. (1980). Differences in the kinetics of dopamine uptake in synaptosome preparations of the median eminence relative to other dopaminergically inervated brain regions. Neuroendocrinology *31*, 316–320.

Beckstead, M.J., Grandy, D.K., Wickman, K., and Williams, J.T. (2004). Vesicular dopamine release elicits an inhibitory postsynaptic current in midbrain dopamine neurons. Neuron *42*, 939–946.

Bedran de Castro, J.C., Khorram, O., and McCann, S.M. (1985). Possible negative ultra-short loop feedback of luteinizing hormone releasing hormone (LHRH) in the ovariectomized rat. Proc. Soc. Exp. Biol. Med. *179*, 132–135.

Berry, S.A., and Gudelsky, G.A. (1991). Effect of D2 dopamine agonists on tuberoinfundibular dopamine neurons. Neuropharmacology *30*, 961–965.

Bikson, M., Hahn, P.J., Fox, J.E., and Jefferys, J.G. (2003). Depolarization block of neurons during maintenance of electrographic seizures. J. Neurophysiol. *90*, 2402–2408.

Björklund, A., and Lindvall, O. (1975). Dopamine in dendrites of substantia nigra neurons: suggestions for a role in dendritic terminals. Brain Res. *83*, 531–537.

Bossé, R., Fumagalli, F., Jaber, M., Giros, B., Gainetdinov, R.R., Wetsel, W.C., Missale, C., and Caron, M.G. (1997). Anterior pituitary hypoplasia and dwarfism in mice lacking the dopamine transporter. Neuron *19*, 127–138.

Bourne, J.A. (2001). SCH 23390: the first selective dopamine D1-like receptor antagonist. CNS Drug Rev. *7*, 399–414.

Briffaud, V., Williams, P., Courty, J., and Broberger, C. (2015). Excitation of tuberoinfundibular dopamine neurons by oxytocin: crosstalk in the control of lactation. J. Neurosci. *35*, 4229–4237.

Brown, R.S., Piet, R., Herbison, A.E., and Grattan, D.R. (2012). Differential actions of prolactin on electrical activity and intracellular signal transduction in hypothalamic neurons. Endocrinology *153*, 2375–2384.

Chase, T.N., Woods, A.C., and Glaubiger, G.A. (1974). Parkinson disease treated with a suspected dopamine receptor agonist. Arch. Neurol. *30*, 383–386.

Clemens, J.A., and Meites, J. (1968). Inhibition by hypothalamic prolactin implants of prolactin secretion, mammary growth and luteal function. Endocrinology *82*, 878–881.

Compton, P.A., Anglin, M.D., Khalsa-Denison, M.E., and Paredes, A. (1996). The D2 dopamine receptor gene, addiction, and personality: clinical correlates in cocaine abusers. Biol. Psychiatry *39*, 302–304.

Cragg, S.J., and Greenfield, S.A. (1997). Differential autoreceptor control of somatodendritic and axon terminal dopamine release in substantia nigra, ventral tegmental area, and striatum. J. Neurosci. *17*, 5738–5746.

Demarest, K.T., and Moore, K.E. (1979a). Comparison of dopamine synthesis regulation in the terminals of nigrostriatal, mesolimbic, tuberoinfundibular and tuberohypophyseal neurons. J. Neural Transm. *46*, 263–277.

Demarest, K.T., and Moore, K.E. (1979b). Lack of a high affinity transport system for dopamine in the median eminence and posterior pituitary. Brain Res. *171*, 545–551.

Demarest, K.T., Riegle, G.D., and Moore, K.E. (1986). The rapid 'tonic' and the delayed 'induction' components of the prolactin-induced activation of tuberoinfundibular dopaminergic neurons following the systemic administration of prolactin. Neuroendocrinology *43*, 291–299.

Demaria, J.E., Nagy, G.M., Lerant, A.A., Fekete, M.I., Levenson, C.W., and Freeman, M.E. (2000). Dopamine transporters participate in the physiological regulation of prolactin. Endocrinology *141*, 366–374.

Dewey, S.L., Smith, G.S., Logan, J., Brodie, J.D., Yu, D.W., Ferrieri, R.A., King, P.T., MacGregor, R.R., Martin, T.P., Wolf, A.P., et al. (1992). GABAergic inhibition of endogenous dopamine release measured in vivo with 11C-raclopride and positron emission tomography. J. Neurosci. *12*, 3773–3780.

Durham, R.A., Johnson, J.D., Moore, K.E., and Lookingland, K.J. (1996). Evidence that D2 receptor-mediated activation of hypothalamic tuberoinfundibular dopaminergic neurons in the male rat occurs via inhibition of tonically active afferent dynorphinergic neurons. Brain Res. *732*, 113–120.

Durham, R.A., Eaton, M.J., Moore, K.E., and Lookingland, K.J. (1997). Effects of selective activation of dopamine D2 and D3 receptors on prolactin secretion and the activity of tuberoinfundibular dopamine neurons. Eur. J. Pharmacol. *335*, 37–42.

Everitt, B.J., Hökfelt, T., Wu, J.Y., and Goldstein, M. (1984). Coexistence of tyrosine hydroxylase-like and gamma-aminobutyric acid-like immunoreactivities in neurons of the arcuate nucleus. Neuroendocrinology *39*, 189–191.

Fedulova, S.A., Kostyuk, P.G., and Veselovsky, N.S. (1985). Two types of calcium channels in the somatic membrane of new-born rat dorsal root ganglion neurones. J. Physiol. *359*, 431–446.

Ford, C.P., Gantz, S.C., Phillips, P.E., and Williams, J.T. (2010). Control of extracellular dopamine at dendrite and axon terminals. J. Neurosci. *30*, 6975–6983.

Freeman, M.E., Kanyicska, B., Lerant, A., and Nagy, G. (2000). Prolactin: structure, function, and regulation of secretion. Physiol. Rev. *80*, 1523–1631.

Fuxe, K. (1963). Cellular localization of monoamines in the median eminence and in the infundibular stem of some mammals. Acta Physiol. Scand. *58*, 383–384.

Geffen, L.B., Jessell, T.M., Cuello, A.C., and Iversen, L.L. (1976). Release of dopamine from dendrites in rat substantia nigra. Nature *260*, 258–260.

Gentet, L.J., and Williams, S.R. (2007). Dopamine gates action potential backpropagation in midbrain dopaminergic neurons. J. Neurosci. *27*, 1892–1901.

Gonzalez, H.A., Kedzierski, W., and Porter, J.C. (1988). Mass and activity of tyrosine hydroxylase in tuberoinfundibular dopaminergic neurons of the aged brain. Control by prolactin and ovarian hormones. Neuroendocrinology *48*, 663–667.

Grace, A.A., and Bunney, B.S. (1986). Induction of depolarization block in midbrain dopamine neurons by repeated administration of haloperidol: analysis using in vivo intracellular recording. J. Pharmacol. Exp. Ther. *238*, 1092–1100.

Grace, A.A., Bunney, B.S., Moore, H., and Todd, C.L. (1997). Dopamine-cell depolarization block as a model for the therapeutic actions of antipsychotic drugs. Trends Neurosci. *20*, 31–37.

Graeff, F.G. (1966). The role of dopamine in motor excitation of mice induced by brain catecholamine releasers. J. Pharm. Pharmacol. *18*, 627–628.

Gruen, P.H., Sachar, E.J., Langer, G., Altman, N., Leifer, M., Frantz, A., and Halpern, F.S. (1978). Prolactin responses to neuroleptics in normal and schizophrenic subjects. Arch. Gen. Psychiatry *35*, 108–116.

Harris, N.C., and Constanti, A. (1995). Mechanism of block by ZD 7288 of the hyperpolarization-activated inward rectifying current in guinea pig substantia nigra neurons in vitro. J. Neurophysiol. *74*, 2366–2378.

Hökfelt, T., and Fuxe, K. (1972). Effects of prolactin and ergot alkaloids on the tubero-infundibular dopamine (DA) neurons. Neuroendocrinology *9*, 100–122.

Holt, R.I., and Peveler, R.C. (2011). Antipsychotics and hyperprolactinaemia: mechanisms, consequences and management. Clin. Endocrinol. (Oxf.) *74*, 141–147.

Ibata, Y., Fukui, K., Okamura, H., Kawakami, T., Tanaka, M., Obata, H.L., Tsuto, T., Terubayashi, H., Yanaihara, C., and Yanaihara, N. (1983). Coexistence of dopamine and neurotensin in hypothalamic arcuate and periventricular neurons. Brain Res. *269*, 177–179.

Jentsch, J.D., Tran, A., Le, D., Youngren, K.D., and Roth, R.H. (1997). Subchronic phencyclidine administration reduces mesoprefrontal dopamine utilization and impairs prefrontal cortical-dependent cognition in the rat. Neuropsychopharmacology *17*, 92–99.

Jiang, Z.G., Pessia, M., and North, R.A. (1993). Dopamine and baclofen inhibit the hyperpolarization-activated cation current in rat ventral tegmental neurones. J. Physiol. *462*, 753–764.

Katz, R.J. (1979). Inhibition-mediating dopamine receptors and the control of intracranial reward. Psychopharmacology (Berl.) *61*, 39–41.

Lacey, M.G., Mercuri, N.B., and North, R.A. (1987). Dopamine acts on D2 receptors to increase potassium conductance in neurones of the rat substantia nigra zona compacta. J. Physiol. *392*, 397–416.

Liang, S.L., and Pan, J.T. (2001). Potent inhibitory effect of selective D2 and D3 agonists on dopamine-responsive dorsomedial arcuate neurons in brain slices of estrogen-primed rats. Life Sci. *69*, 2653–2662.

Liang, S.L., Hsu, S.C., and Pan, J.T. (2014). Involvement of dopamine D2 receptor in the diurnal changes of tuberoinfundibular dopaminergic neuron activity and prolactin secretion in female rats. J. Biomed. Sci. *21*, 37.

Lin, J.Y., Yen, S.H., Shieh, K.R., Liang, S.L., and Pan, J.T. (2000). Dopamine and 7-OH-DPAT may act on D(3) receptors to inhibit tuberoinfundibular dopaminergic neurons. Brain Res. Bull. *52*, 567–572.

Lippa, A.S., Antelman, S.M., Fisher, A.E., and Canfield, D.R. (1973). Neurochemical mediation of reward: a significant role for dopamine? Pharmacol. Biochem. Behav. *1*, 23–28.

Lookingland, K.J., Jarry, H.D., and Moore, K.E. (1987). The metabolism of dopamine in the median eminence reflects the activity of tuberoinfundibular neurons. Brain Res. *419*, 303–310.

Lyons, D.J., and Broberger, C. (2014). TIDAL WAVES: Network mechanisms in the neuroendocrine control of prolactin release. Front. Neuroendocrinol. *35*, 420–438.

Lyons, D.J., Horjales-Araujo, E., and Broberger, C. (2010). Synchronized network oscillations in rat tuberoinfundibular dopamine neurons: switch to tonic discharge by thyrotropin-releasing hormone. Neuron *65*, 217–229.

Lyons, D.J., Hellysaz, A., and Broberger, C. (2012). Prolactin regulates tuberoinfundibular dopamine neuron discharge pattern: novel feedback control mechanisms in the lactotrophic axis. J. Neurosci. *32*, 8074–8083.

MacLeod, R.M., and Lehmeyer, J.E. (1974). Studies on the mechanism of the dopamine-mediated inhibition of prolactin secretion. Endocrinology *94*, 1077–1085.

Madhusoodanan, S., Parida, S., and Jimenez, C. (2010). Hyperprolactinemia associated with psychotropics–a review. Hum. Psychopharmacol. *25*, 281–297.

Marrion, N.V., and Tavalin, S.J. (1998). Selective activation of Ca2+-activated K+ channels by co-localized Ca2+ channels in hippocampal neurons. Nature *395*, 900–905.

Momiyama, T., Todo, N., and Sasa, M. (1993). A mechanism underlying dopamine D1 and D2 receptor-mediated inhibition of dopaminergic neurones in the ventral tegmental area in vitro. Br. J. Pharmacol. *109*, 933–940.

Nowycky, M.C., Fox, A.P., and Tsien, R.W. (1985). Three types of neuronal calcium channel with different calcium agonist sensitivity. Nature *316*, 440–443.

Paladini, C.A., Robinson, S., Morikawa, H., Williams, J.T., and Palmiter, R.D. (2003). Dopamine controls the firing pattern of dopamine neurons via a network feedback mechanism. Proc. Natl. Acad. Sci. USA *100*, 2866–2871.

Piotte, M., Beaudet, A., Joh, T.H., and Brawer, J.R. (1985). The fine structural organization of tyrosine hydroxylase immunoreactive neurons in rat arcuate nucleus. J. Comp. Neurol. *239*, 44–53.

Reavill, C., Bond, B., Overend, P., and Hunter, A.J. (1993). Pharmacological characterization of the discriminative stimulus properties of the dopamine D1 agonist, SKF 81297. Behav. Pharmacol. *4*, 135–146.

Reeves, S.J., Grasby, P.M., Howard, R.J., Bantick, R.A., Asselin, M.C., and Mehta, M.A. (2005). A positron emission tomography (PET) investigation of the role of striatal dopamine (D2) receptor availability in spatial cognition. Neuroimage *28*, 216–226.

Richards, C.D., Shiroyama, T., and Kitai, S.T. (1997). Electrophysiological and immunocytochemical characterization of GABA and dopamine neurons in the substantia nigra of the rat. Neuroscience *80*, 545–557.

Seeman, P. (2013). Schizophrenia and dopamine receptors. Eur. Neuropsychopharmacol. *23*, 999–1009.

Serretti, A., and Chiesa, A. (2011). A meta-analysis of sexual dysfunction in psychiatric patients taking antipsychotics. Int. Clin. Psychopharmacol. *26*, 130–140.

Servan-Schreiber, D., Bruno, R.M., Carter, C.S., and Cohen, J.D. (1998). Dopamine and the mechanisms of cognition: Part I. A neural network model predicting dopamine effects on selective attention. Biol. Psychiatry *43*, 713–722.

Silva, N.L., and Bunney, B.S. (1988). Intracellular studies of dopamine neurons in vitro: pacemakers modulated by dopamine. Eur. J. Pharmacol. *149*, 307–315.

Södersten, E., Feyder, M., Lerdrup, M., Gomes, A.L., Kryh, H., Spigolon, G., Caboche, J., Fisone, G., and Hansen, K. (2014). Dopamine signaling leads to loss of Polycomb repression and aberrant gene activation in experimental parkinsonism. PLoS Genet. *10*, e1004574.

Stevens, J., Wilson, K., and Foote, W. (1974). GABA blockade, dopamine and schizophrenia: experimental studies in the cat. Psychopharmacology (Berl.) *39*, 105–119.

Timmerman, W., Deinum, M.E., Westerink, B.H., and Schuiling, G.A. (1995). Lack of evidence for dopamine autoreceptors in the mediobasal hypothalamus: a microdialysis study in awake rats. Neurosci. Lett. *195*, 113–116.

Ungless, M.A., Argilli, E., and Bonci, A. (2010). Effects of stress and aversion on dopamine neurons: implications for addiction. Neurosci. Biobehav. Rev. *35*, 151–156.

Vandael, D.H., Ottaviani, M.M., Legros, C., Lefort, C., Guérineau, N.C., Allio, A., Carabelli, V., and Carbone, E. (2015). Reduced availability of voltage-gated sodium channels by depolarization or blockade by tetrodotoxin boosts burst firing and catecholamine release in mouse chromaffin cells. J. Physiol. *593*, 905–927.

Westermann, K.H., and Staib, A.H. (1976). [Nigrostriatally induced motor reactions in the rat. I. Rotational behavior and posture asymetry after intracerebral injection of apomorphine and dopamine]. Acta Biol. Med. Ger. *35*, 773–780.

Wong, A.Y., Borduas, J.F., Clarke, S., Lee, K.F., Béïque, J.C., and Bergeron, R. (2013). Calcium influx through N-type channels and activation of SK and TRP-like channels regulates tonic firing of neurons in rat paraventricular thalamus. J. Neurophysiol. *110*, 2450–2464.

Xu, C., Roepke, T.A., Zhang, C., Rønnekleiv, O.K., and Kelly, M.J. (2008). Gonadotropin-releasing hormone (GnRH) activates the m-current in GnRH neurons: an autoregulatory negative feedback mechanism? Endocrinology *149*, 2459–2466.

Cell Reports, Volume *15*

Supplemental Information

Dopamine Autoreceptor Regulation of a Hypothalamic Dopaminergic Network

Stefanos Stagkourakis, Hoseok Kim, David J. Lyons, and Christian Broberger

SUPPLEMENTAL INFORMATION

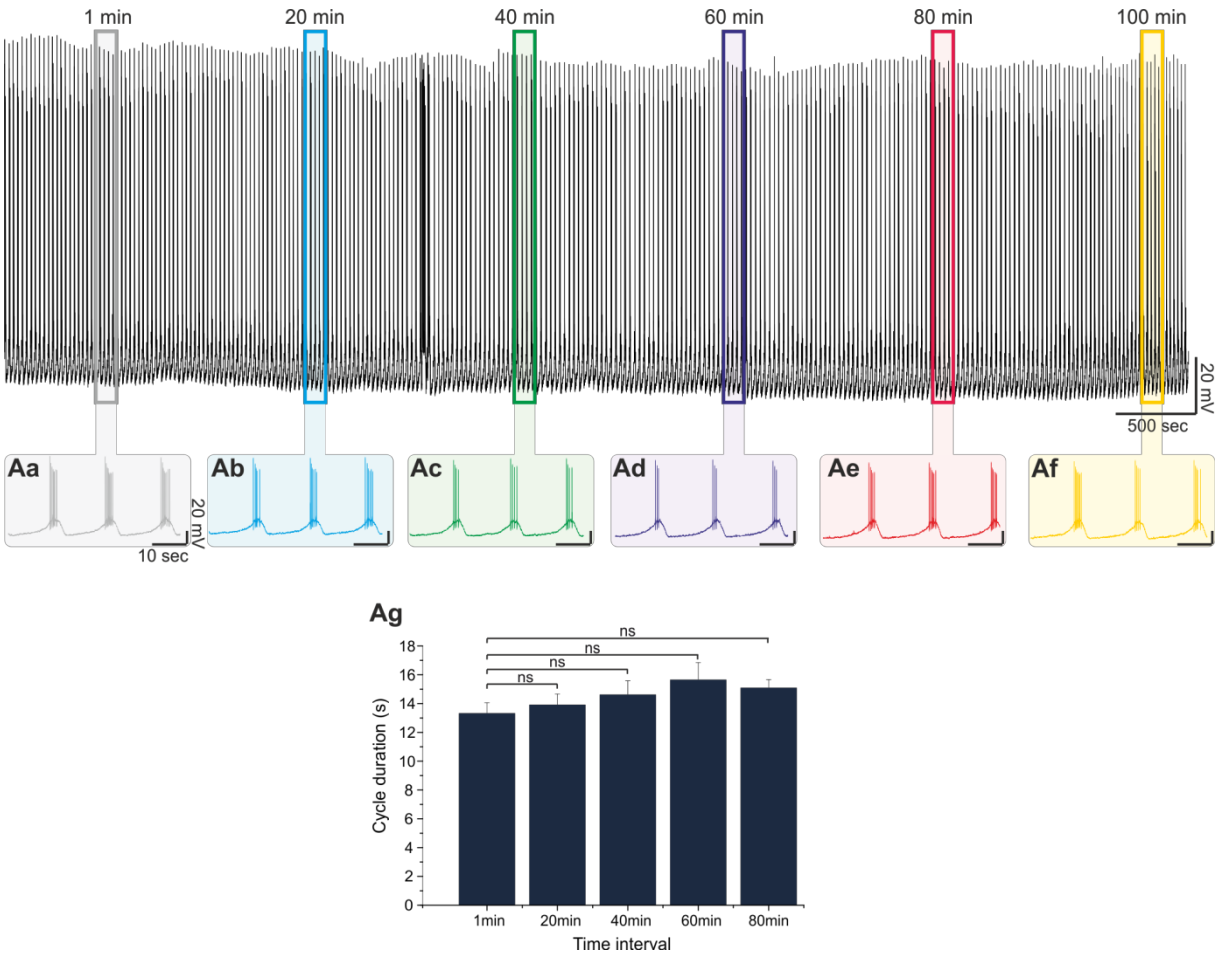

Figure S1. Robustness of the TIDA oscillation and maintenance of rhythmicity in long whole-cell recordings, see Experimental Procedures.

(Aa-g) Cycle duration does not change in control long-term recordings (+0.71±0.55 s; p>0.05 at t=40 min vs t=1 min; n=6). **(Ag)** Cycle duration does not change in control long-term recordings in an 80 min period (+0.97±1.03 s; p>0.05 at t=80 min vs t=1 min; n=3).

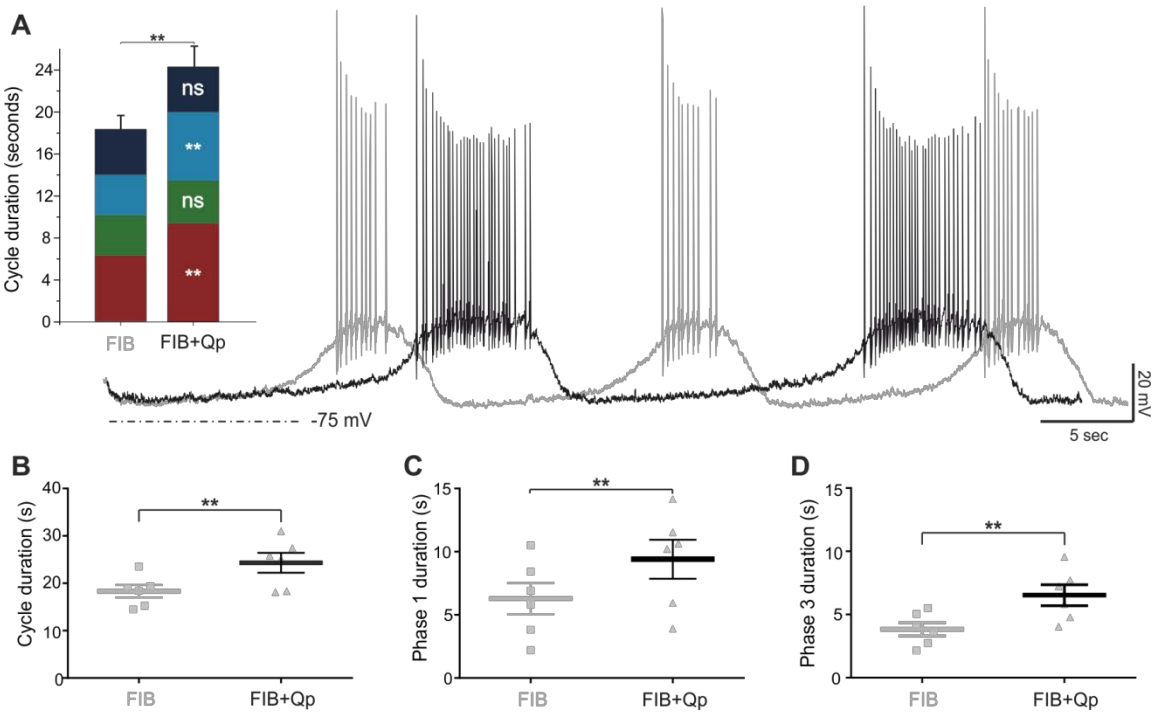

Figure S2. Related to Figure 1; D2R activation effect on cycle and phase duration persists in fast ionotropic blockade.

(A) Quinpirole application leads to an increase in cycle duration in the presence of fast ionotropic blockade (FIB; Picrotoxin 100 μM, CNQX 10 μM and AP-5 25 μM) via phase 1 and phase 3 prolongation. **(B)** Cycle duration increase (+5.99±0.91 s; $p<0.01$ *vs* FIB; n=6). **(C)** Phase 1 duration increase (+3.12±0.52 s; $p<0.01$ *vs* FIB; n=6). **(D)** Phase 3 duration increase (+2.69±0.47 s; $p<0.01$ *vs* FIB; n=6).

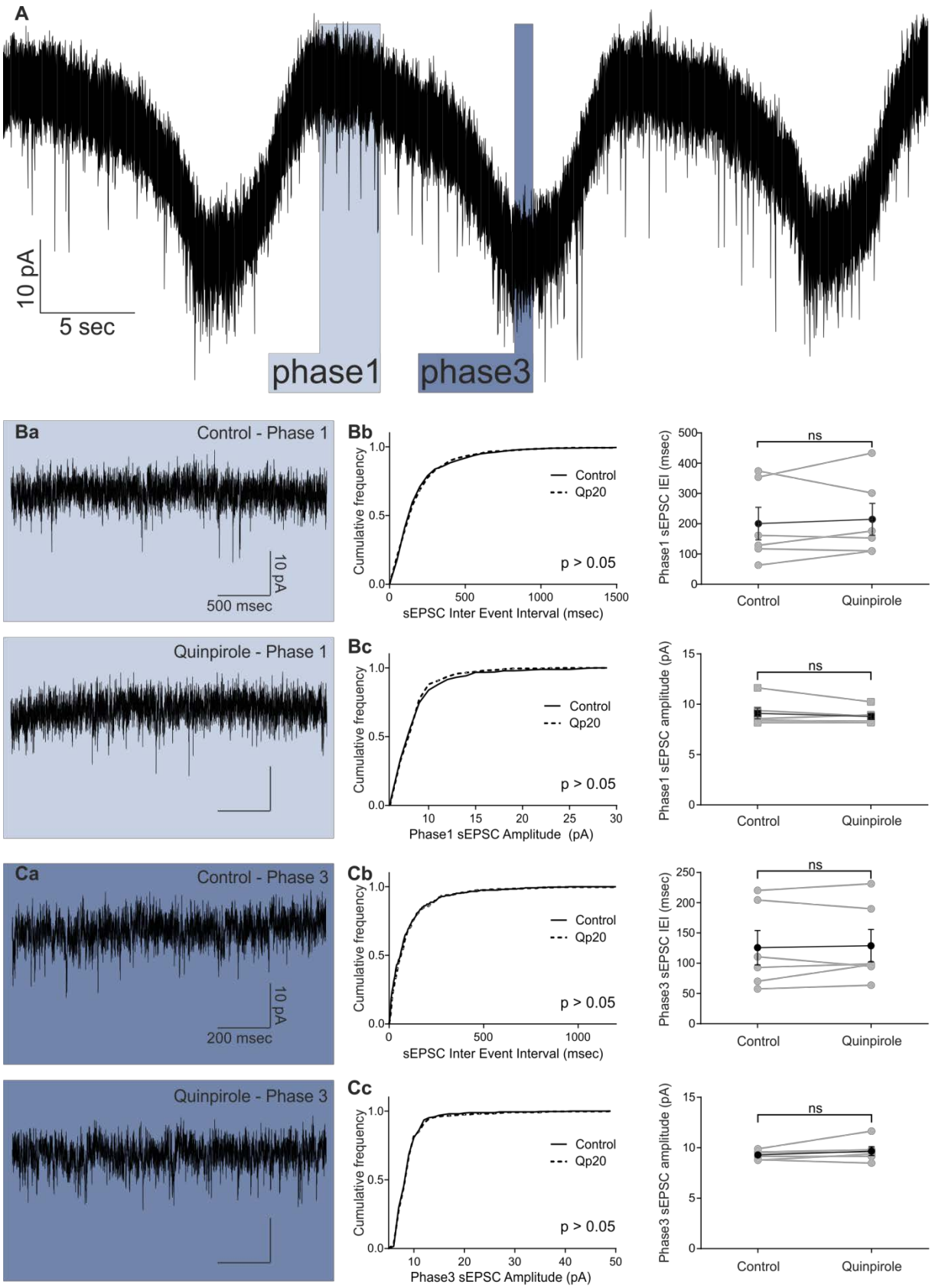
A
10 pA
5 sec
phase1
phase3
Ba
Control - Phase 1
10 pA
500 msec
Bb
Cumulative frequency
Control
Qp20
p > 0.05
sEPSC Inter Event Interval (msec)
Phase1 sEPSC IEI (msec)
ns
Control
Quinpirole
Quinpirole - Phase 1
Bc
Phase1 sEPSC Amplitude (pA)
Phase1 sEPSC amplitude (pA)
Ca
Control - Phase 3
200 msec
Cb
Phase3 sEPSC IEI (msec)
Quinpirole - Phase 3
Cc
Phase3 sEPSC Amplitude (pA)
Phase3 sEPSC amplitude (pA)

20

21

22

Figure S3. Related to Figure 5; Spontaneous EPSCs are not affected by D2R activation.

(Aa) Raw voltage clamp trace demonstrating the time intervals from which sEPSCs were sampled during phase 1 (light blue) and phase 3 (dark blue). (Ba) Raw voltage clamp traces in control *vs* quinpirole illustrating no change in sEPSC frequency or amplitude during phase 1. (Bb) Cumulative frequency distribution of sEPSC inter-event interval demonstrating no difference in frequency (+14.18±22.30 ms, KS-2 $p<0.05$; *t*-test $p<0.05$; n=5) or amplitude (Bc) (-0.29±0.25 pA, KS-2 $p>0.05$; *t*-test $p>0.05$; n=5) during phase 1. (Ca) Raw voltage clamp trace illustrating no difference in frequency or amplitude of sEPSCs during phase 3 after quinpirole application. (Cb) Cumulative frequency distribution of sEPSC inter event interval demonstrating no difference in frequency (+3.28±6.73 ms, KS-2 $p<0.05$; *t*-test $p<0.05$; n=5) or amplitude (Cc) (+0.38±0.30 pA, KS-2 $p>0.05$; *t*-test $p>0.05$; n=5) during phase 3.

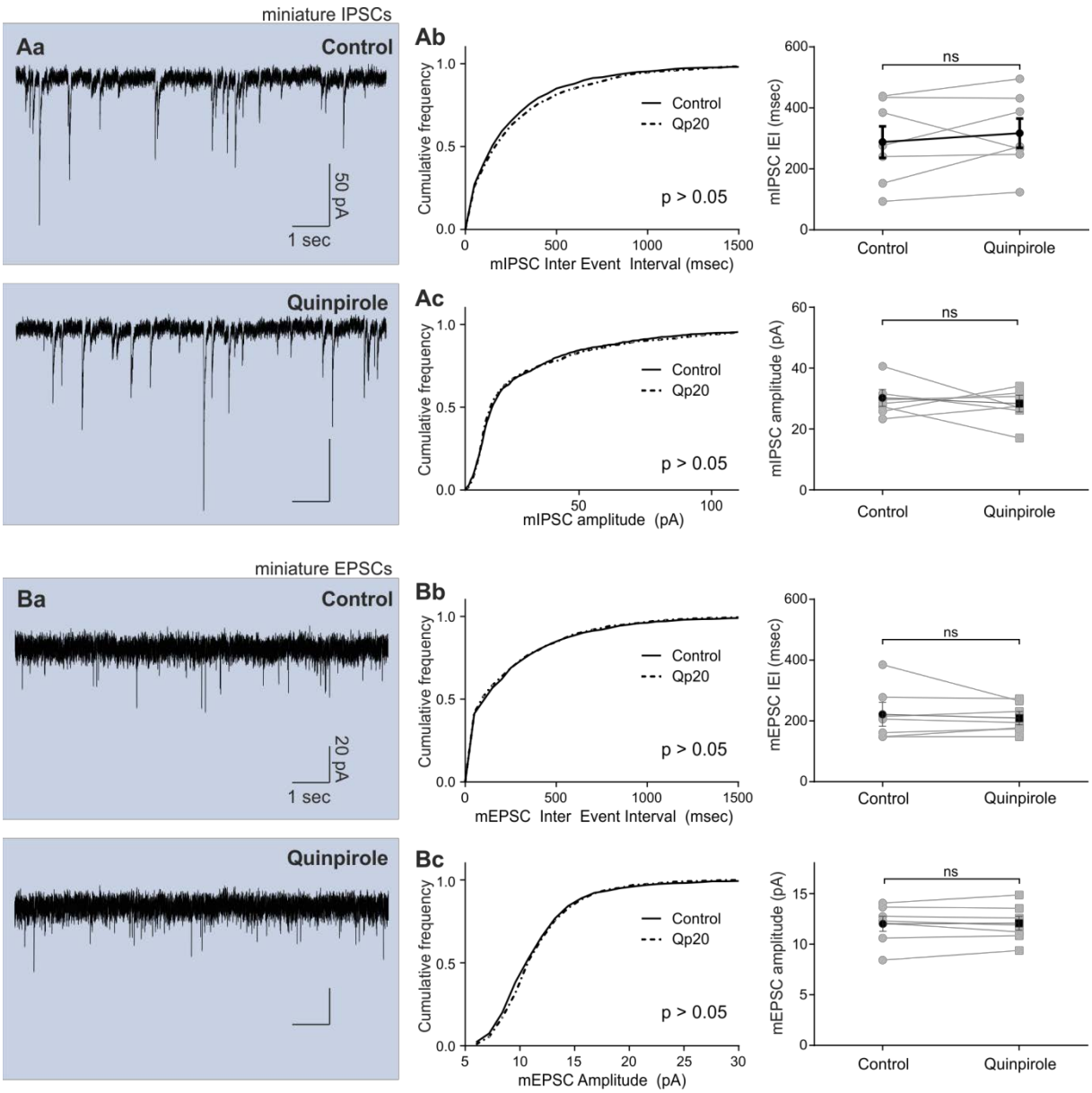

FigureS4. Related to Figure 5; Miniature synaptic transmission is unaffected by D2R activation in TIDA neurons.

(Aa) Raw voltage clamp traces in control *vs* quinpirole illustrating no change in miniature IPSC frequency or amplitude. (Ab) Cumulative frequency distribution of mIPSC inter-event interval demonstrating no difference in frequency (+29.07±30.56 ms, KS-2 $p<0.05$; *t*-test $p<0.05$; n=7) or amplitude (Ac) (-1.78±3.07 pA, KS-2 $p>0.05$; *t*-test $p>0.05$; n=7). (Ba) Raw voltage clamp trace illustrating no difference in frequency or amplitude of mEPSCs as a result of quinpirole application. (Bb) Cumulative frequency distribution of mEPSC inter-event interval demonstrating no difference in frequency (-10.75±18.73 ms, KS-2 $p<0.05$; *t*-test $p<0.05$; n=7) or (Bc) amplitude (+0.06±0.24 pA, KS-2 $p>0.05$; *t*-test $p>0.05$; n=7).

Table S2. Related to Figure 2 Ac-Ad and Bc-Bd; D2R antagonists decrease the amplitude and broaden the TIDA action potentials.

		Control	Eticlopride 1 μM
Amplitude (mV)	AP1	97.41 ± 1.12	85.83 ± 2.05 **
	AP2	85.87 ± 1.79	71.77 ± 2.19 **
	AP3	79.74 ± 1.43	61.55 ± 3.86 **
	AP4	75.35 ± 1.65	57.79 ± 3.36 **
	AP5	72.35 ± 1.54	54.34 ± 3.01 **
Half-width (ms)	AP1	1.49 ± 0.10	1.56 ± 0.09
	AP2	1.74 ± 0.14	1.93 ± 0.14 **
	AP3	1.91 ± 0.16	2.36 ± 0.26 *
	AP4	2.08 ± 0.18	2.54 ± 0.25 **
	AP5	2.17 ± 0.18	2.79 ± 0.39 *

		Control	Haloperidol 1 μM
Amplitude (mV)	AP1	95.09 ± 1.91	89.11 ± 2.26 **
	AP2	85.00 ± 2.28	76.82 ± 2.76 **
	AP3	79.73 ± 2.93	68.85 ± 2.94 ***
	AP4	74.38 ± 2.25	63.95 ± 2.77 **
	AP5	74.16 ± 2.44	59.28 ± 2.13 **
Half-width (ms)	AP1	1.37 ± 0.02	1.41 ± 0.04
	AP2	1.53 ± 0.04	1.63 ± 0.04 *
	AP3	1.67 ± 0.06	1.82 ± 0.05 **
	AP4	1.79 ± 0.06	1.97 ± 0.07 **
	AP5	1.82 ± 0.07	2.14 ± 0.07 **

SUPPLEMENTAL EXPERIMENTAL PROCEDURES

Ca^{2+} current studies. To examine modulation of Ca^{2+} channels, bath application of TTX (0.5μM) was used to block the voltage-gated Na^{+} conductance (Cohen et al., 1981) and Ba^{2+} (1mM) was added to the extracellular solution to augment the Ca^{2+} channel currents (Kostiuk et al., 1985, Smith et al., 1986). The Cs^{+}-based intracellular solution described for recordings of EPSCs (see above) was used to block K^{+} currents (Adelman and Senft, 1966, Clay and Shlesinger, 1984). At the end of every experiment $CdCl_2$ (400 μM) was applied to abolish the Ca^{2+} conductances (Thevenod and Jones, 1992, Swandulla and Armstrong, 1989); that recording was used as the negative control. Due to incomplete blockade of the K^{+} leak conductance by Cs^{+}, the Cd^{2+} trace was subtracted digitally from Ca^{2+} recordings of the same neuron. Run-down of Ca^{2+} currents was minimized by using the Cs^{+}-based intracellular solution (Zhang et al., 1994), by applying brief (150 ms) ramp protocols adapted from (Chen and Kirchgessner, 2002), and by waiting for 10 mins between activating currents, a time interval that was used for pharmacological reagents to reach a peak of effect. In these conditions, run-down of the HVA Ca^{2+} current was calculated to be 3.3±0.69% per 10 min (n=3). The values of all Ca^{2+} peak currents were corrected based on the run-down estimate.

Oscillation phase analysis. We developed a Matlab script in order to isolate the contribution of each phase to the oscillation cycle duration. The stereotyped traits of the oscillation were used to develop an algorithm, to allow analysis of duration and membrane voltage of the four phases of the duty cycle. Four phases were defined on the basis of slope (dV/dt) changes (Figure 1A): Phase 1 was defined as the slow depolarizing phase beginning at the nadir of the membrane potential (the lowest mV value of an oscillation cycle) and ending within a time window of 0.5-4sec prior to the first action potential of the oscillation cycle, where the point of maximal change in slope defines the phase 2 initiation point. Phase 2 was thus defined as the fast depolarizing phase beginning at the phase 2 initiation point and ending at the firing threshold (defined as dV/dt>5 mV/ms) of the first action potential of the oscillation cycle. Phase 3 was defined as the action potential firing plateau phase, extending between the firing threshold of the first action potential of the oscillation cycle until the end of firing where the maximal change in slope defines the end of phase 3 and beginning of phase 4. Phase 4 constitutes the fast hyperpolarizing phase between end of phase 3 and the ensuing nadir point.

Recording of EPSCs and IPSCs. In recordings of sIPSCs and mIPSCs whole-cell voltage-clamp recordings were performed with micropipettes filled with intracellular solution containing (in mM), 150 KCl, 10 HEPES, 10 EGTA, and 2 Na_2ATP, pH 7.3 (with KOH), in the presence of fast excitatory neurotransmission blockade by CNQX (10 μM) and AP-5 (25 μM). The final part of every s/mIPSCs recording was application of picrotoxin (100 μM) and the observation of complete loss of all synaptic events. In recordings of sEPSCs and mEPSCs whole-cell voltage-clamp recordings were performed with micropipettes filled with intracellular solution containing (in mM), 140 K-gluconate, 10 KCl, 10 HEPES, 10 EGTA, and 2 Na_2ATP, pH 7.3 (with KOH), in the presence of fast inhibitory neurotransmission blockade by picrotoxin (100 μM). The final part of every s/mEPSCs recording was application of picrotoxin (100 μM) and the observation of complete loss of all synaptic events. sIPSCs and sEPSCs along phases were compared via manual selection. Beginning of phase 1 in voltage-clamp was defined as the most positive point (in pA), of a new oscillation cycle and beginning of phase 3 was selected as the most negative point (in pA) of the oscillation cycle.

*Reagents***.** Dopamine hydrochloride, apomorphine hydrochloride hydrate, picrotoxin, cadmium chloride, haloperidol, $BaCl_2$ and (TEA)-Cl_2 were purchased from Sigma. TTX and charybdotoxin were purchased from Alomone Labs. (-)-quinpirole hydrochloride, SKF-81297 hydrobromide, (-)-Eticlopride hydrochloride, CNQX, AP-5, nimodipine and CGP 55845 hydrochloride were purchased from Tocris Bioscience. GVIA ω-conotoxin was purchased from Abcam biochemical.